Inter-compartment concentration monitoring of key species in a vanadium redox flow cell operating with and without polarization: Experiments and construction of a predictive model

Toussaint Ntambwe Kambuyi, Fabien Chauvet, Brigitte Dustou, Théo Tzedakis

Inter-compartment concentration monitoring of key species in a vanadium redox flow cell operating with and without polarization: experiments and construction of a predictive model

Toussaint Ntambwe Kambuyi, Fabien Chauvet*, Brigitte Dustou, Théo Tzedakis*

Laboratoire de Génie Chimique, Université de Toulouse, CNRS, INPT, UT3, Toulouse, France

*Corresponding authors: fabien.chauvet@univ-tlse3.fr and theodore.tzedakis@univ-tlse3.fr

Abstract

The usually encountered phenomenon of vanadium crossover in Vanadium Redox Flow Batteries (VRFB), leading to energy capacity losses, is specifically studied without (diffusion measurements) and with the application of an electric current (battery operating conditions). The experimental set-up is an electrochemical filter-press reactor integrating a Nafion^{TM} 424 membrane and two storage tanks. The electrolytes composition on both sides was determined using potentiometric titration (VO_2^+ and H^+) and UV-Vis analysis (V^{2+}, V^{3+} and VO^{2+}). First, experiment is conducted without polarization and a model based on mass balance equation incorporating diffusion flux and electrolyte volumes change is derived to predict electrolytes composition on both sides. The effective diffusion coefficient of VO^{2+} in the membrane is obtained by fitting the model with experimental data. The experiment is then carried out under galvanostatic polarization (10 mA/cm^2) and a model embedding, simultaneously, electrolyte volumes variation, diffusion and migration across the membrane and the electrochemical and self-discharge reactions, is proposed to predict electrolytes composition. The partitioning of the applied current between all possible electrochemical reactions is addressed using a specific algorithm based on logical tests on limiting currents. The resulting system of coupled ordinary differential equations is solved numerically using standard python functions. The results indicate a satisfactory agreement between predicted and experimental data and highlight the requirement of considering all phenomena for an accurate prediction of electrolytes composition in VRFB. The interest of applying the developed model to simulate and predict composition evolution in VRFB (State of Charge (SoC) and acidity) is discussed.

Keywords: Redox Flow Batteries, Vanadium Crossover, Modelling, Transport, Self-discharge, Proton Exchange Membranes.

Nomenclature	
A	: absorbance
c	: concentration (mol/m^3)
V_j	: electrolyte volume on j side (m^3)
J	: mass flux (mol/s)
S	: electrode surface area (m^2)
S_m	: membrane surface area (m^2)
D	: diffusion coefficient (m^2/s)
L	: membrane thickness (m)
F	: Faraday constant (96,485 c/mol)
z	: valence
u	: ionic mobility (mol/s/kg)
E	: electric field (V/m)
R	: universal gas constant (8.314 J/mol/K)
T	: absolute temperature (293.15 K)
ΔV_m	: potential drop across the membrane (V)
I	: current applied (A)
t^{H^+}	: transference number of protons
R_m	: resistance of the membrane (Ω)
I_{lim}	: limiting current (A)
k_c	: mass transfer coefficient (m/s)
r	: reaction rate (mol/m^3/s)
k	: rate constant of self-discharge reaction (s^{-1})
Superscripts	

i	: refers to « oxidation state of vanadium ion »
II	: refers to « vanadium (II) ion (V^{2+}) »
III	: refers to « vanadium (III) ion (V^{3+}) »
IV	: refers to « vanadium (IV) ion (VO^{2+}) »
V	: refers to « vanadium (V) ion (VO_2^{+}) »
H^+	: refers to « ion proton »
W	: refers to the « water »
Subscripts	
v:	: refers to the « vanadium side »
s	: refers to the « sulfuric acid side »
p	: refers to the « posolyte »
n	: refers to the « negolyte »
in	: refers to the « inlet »
out	: refers to the « outlet »
D	: refers to the « diffusion »
M	: refers to the « migration »
m	: refers to the « membrane »
$elec$	: refers to the « electrochemical reaction »
Greek letters	
σ_m	: membrane conductivity (0.083 $S.m^{-1}$)
α	: net mass flux of self-discharge reaction ($mol.s^{-1}$)

1. Introduction

Renewable energy sources, including solar and wind, are considered as one of the safe ways to produce electric energy with sustainability. However, these resources are intermittent and discontinuous, resulting in an instability in energy production unable to adequately meet demand. Thus, an Energy Storage System (ESS), allowing the storage of electrical energy from renewable sources (solar or wind) and its release on demand, is mandatory for a successful implementation of renewable energy in electrical grid applications. VRFB are one of the most suitable candidates for this purpose as it offers many advantages over conventional batteries such as long lifecycles (no cross-contamination issues), high safety (aqueous solutions) and environmentally friendly (recyclable species) [1–8]. In a typical set-up, the VRFB consists of:

- an electrochemical cell integrating two inert current collectors (electrodes) and an ion exchange membrane
- two separated external tanks for electrolyte storage.

The electrolytes are pumped through the electrochemical cell where electrochemical reactions occur on electrodes surface [1,9,10]. The fact the storage tanks are separated from the electrochemical cell constitutes a prominent feature of the Redox Flow Batteries (RFBs) as it allows power output and storage capacity to be independently tailored and therefore make it possible to separately scale up the energy storage capacity and power capability as needed [1]. The membrane acts as a selective barrier which ideally allows only the transport of protons, while preventing the cross-diffusion of other species contained in electrolyte solutions from the two tanks. The most often used membrane in RFBs applications is Nafion® (a perfluorosulfonic acid (PFSA)) thanks to its high chemical and mechanical stability and its fair proton conductivity. However, Nafion membrane can lead to a crossover of species contained in electrolytes resulting in contamination issues. In the case of VRFB, the contamination issues due to the crossover mechanism are avoided as this system employs the same element

(vanadium) in four oxidation states (V^{2+}, V^{3+} for the negolyte and VO^{2+} and VO_2^+ for the posolyte) [1,4,11,12]. However, crossover in VRFB can lead to the self-discharge reactions, resulting in a loss of energy capacity [13–15]. Additionally, the water is also transported through Nafion during battery operation, which affects all concentrations into the battery. Thus, many efforts are being conducted to suppress or reduce the vanadium ions and the water permeation rates [16–20]. Besides, transport mechanisms across Nafion membrane, including vanadium ions and water transport, were investigated employing experimental methods and/or numerical models and in the systems with or without polarization. The various methods used to monitor the composition of the tanks (UV-Vis analysis, conductivity, redox potential, viscosity measurements, etc.), and thus the SoC, are summarized in recent reviews [21,22]. Sun and co-workers [23], investigated water transport and vanadium ions crossover through Nafion® 115 membrane in a dialysis cell (without applying an electric field); using simple mass balance equation based on Fick's law, the authors have determined the effective diffusion coefficients of the different vanadium ions in the Nafion membrane. Likewise, You et al. proposed a model to predict the self-discharge process in a kilowatt-class stack of VRFB at different State of Charge (SoC) taking into account the variation of electrolyte volume [24]. As for water transport, Mohammedi et al. [15] and Sukkar and Skyllas-kazacos [14] carefully conducted experimental studies on water transport across various commercial ion exchange membranes without polarization. The tanks composition was recently monitored *in situ* (avoids sampling and therefore allows a finer measurement of the capacity loss due to crossover) during VRFB operation by amperometric and electrochemical quartz crystal microbalance measurements [25] and by measurement of the refractive index of electrolytes [26].

Skyllas-Kazacos and Goh used an all-vanadium redox flow battery with discharging/charging at constant current and developed a simple model based on mass balance equations and effective diffusion coefficients of different vanadium ions in Nafion to determine the

concentration profiles of different vanadium ions [27]. Tang et al. developed a model incorporating mass and energy balances to investigate the thermal effect of self-discharge on electrolyte temperature [28]. Oh et al. developed a model which considers: i) the water production/consumption by the electrochemical reactions involving VO^{2+}/VO_2^+ and also by the side reactions (water electrolysis), and ii) the various mechanisms of water crossover through the membrane arising from diffusion, Electro-Osmotic Drag (EOD), and vanadium crossover with bound water [29]. Vanadium transport mechanisms have also been modelled in other similar works [30–34]. With an alternative approach, Hayer and Kohns [35] showed that activity coefficients must be taken into account to correctly predict the equilibrium part of the cell voltage, i.e. the Open Cell Voltage (OCV). This is critical in works where the study of the capacity loss is based on the comparison between a cell voltage relationship and experimentally measured cell voltage.

However, to date, the bibliography does not exhibit any model that incorporates simultaneously all the phenomena. For instance, most of the developed models, dealing with the determination of effective diffusion coefficients, do not take into account the water transport (the electrolyte volume is considered “constant”) and this affects the prediction accuracy of the concentration profiles as water transport leads to dilute one side while enrich the other side. In addition, the monitoring of sulfuric acid concentration in the system is rarely performed in works dealing with vanadium crossover and water transport in VRFB. Indeed, the acidity, which is affected by several mechanisms in VRFB (electrochemical reactions, self-discharge reactions, water transport and H^+ ions migration), can affect electrolyte stability (precipitation) and therefore the concentration of dissolved vanadium species within the system.

Another critical point is that, when VRFB is operating (charge or discharge), the partitioning of the electric current between all possible electrochemical reactions (Rx. II-IX),

as well as the coupling with the self-discharge reactions (Rx. X-XII), is not accurately described by any model. These couplings affect the temporal evolution of the concentration of vanadium species and therefore the SoC of the battery.

The aim of this paper is to perform an in-depth study of vanadium transport mechanisms occurring within the reactor as well as the resulting variation in electrolytes composition in storage tanks, including acid concentration, vanadium species concentration and electrolyte volume variation. This is achieved by the construction of a model which embeds simultaneously mass balance equations, transport flux through the membrane (vanadium ions, water and acid), electrochemical and self-discharge reactions. Two different cases were studied: case A without polarization (I = 0) and case B with galvanostatic polarization. For both cases, the experimental measurements are carried out using a lab-scale electrochemical filter-press reactor coupled with two storage tanks, including the monitoring of vanadium ions and acid concentrations, as well as water inter-compartment flux. The model predictions are validated using experimental measurements and the application of the proposed model to VRFB is discussed.

2. Material and methods

2.1. Experimental set-up

Figure 1 shows a sketch of the experimental set-up used in this study, which includes the electrochemical cell, storage tanks (Borosilicate® glass volumetric cylinders), peristaltic pumps and tubing (Masterflex® L/S®18).

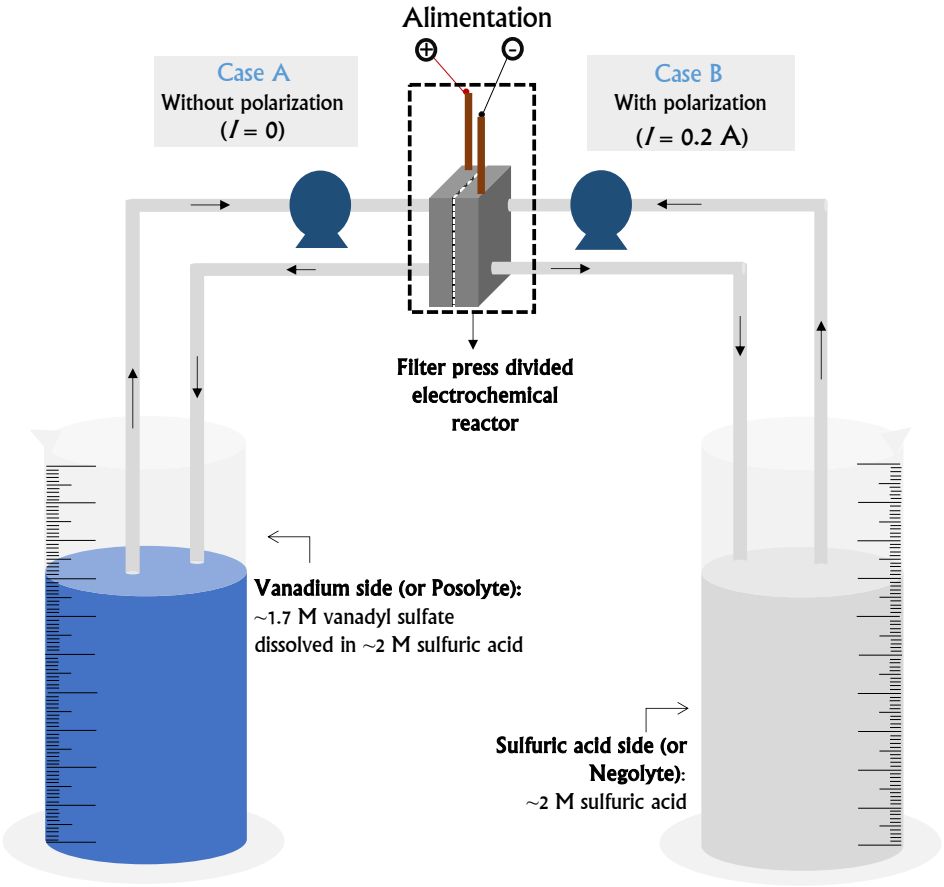

Figure 1: Schematic representation of the experimental set-up.

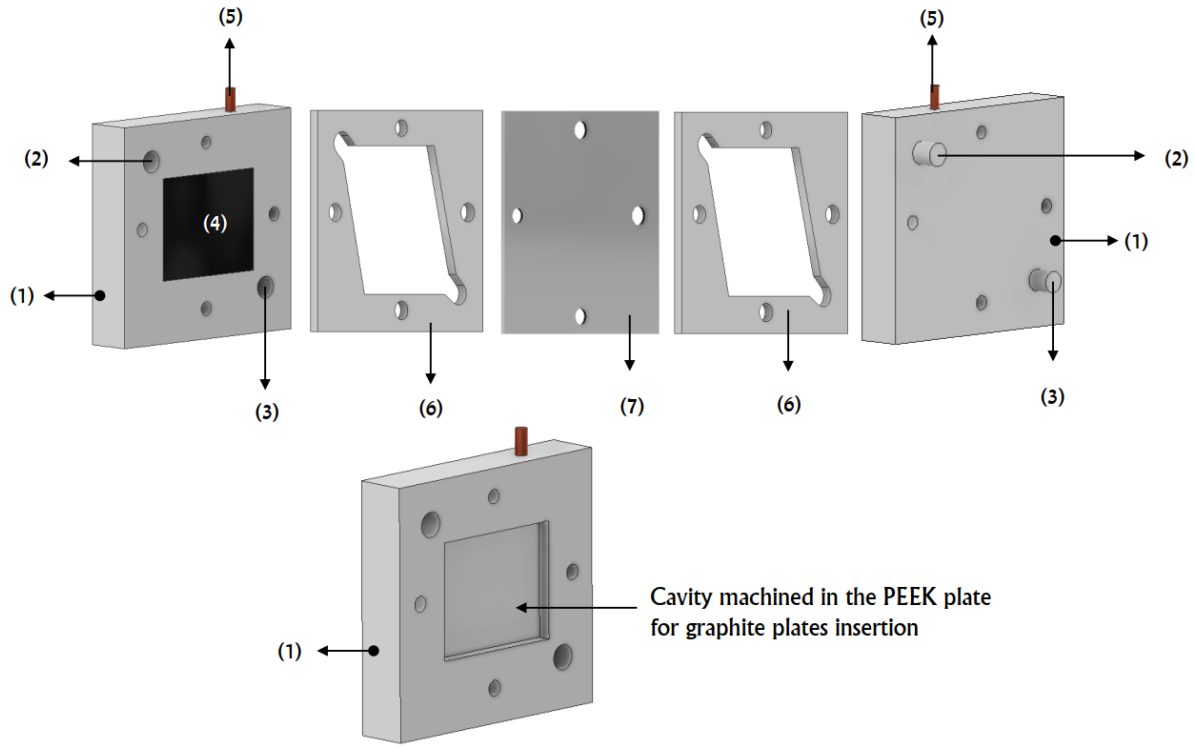

Figure 2 : Components of the divided filter press electrochemical reactor used in this work: (1) PEEK plates; (2) inlet of the electrolytes; (3) outlet of the electrolytes; (4) graphite plates (working electrodes) with 20 cm^2 of active surface area inserted in PEEK plates; (5) Cooper rods (electrical connectors) crossing the PEEK plate and screwed on the side face of the graphite plate; (6) Silicone gaskets, (7) Nafion™ 424 membrane. The remaining four circles on the PEEK plates (1), silicon gaskets (6) and membrane (7) correspond to the holes in which screws are introduced to assemble the system and avoid leakages.

As sketched in Figure 2, the electrochemical cell is a filter press reactor assembled by sandwiching the membrane between two silicone gaskets (3 mm of thickness) and two polyetheretherketone (PEEK) housings (85 × 95 × 30 mm). The silicone gaskets placed on each side of the membrane define the electrolytic compartments which the volume is approximately equal to 8 cm^3. The internal face of the PEEK was machined to create a cavity in which the electrodes (graphite plates, effective surface area of 20 cm^2) were inserted, as indicated in Figure 2. The remaining openings were filled with epoxy resin (Araldite) to prevent any electrolyte infiltration during experiment. Nafion™ 424 (Ion power, GmbH, Germany) with a polytetrafluoroethylene (PTFE) fibber reinforcement was employed as membrane separating

the electrolytic compartments; the working surface area of the membrane is the same as the one of the electrodes (20 cm^2). The Nafion™ 424 membrane is a dense (without macro-porosity) cation exchange membrane and its average thickness is 200 µm. This membrane was selected mainly for its mechanical resistance that allows the assembly of the filter-press reactor without risks of damages (rips). Furthermore, when the reactor is operating, potential damages by the imposed flow are also avoided. In Figure 1, the left storage tank (which will be called "vanadium" side or posolyte) is initially filled with a vanadium solution containing approximatively 1.7 M of vanadium IV ions, VO^{2+}, in 2 M H_2SO_4. The vanadium solution was prepared by dissolving $VOSO_4.nH_2O$ commercial salt (Chemos GmbH&Co.KG, 99%) in 2 M sulfuric acid (BDH® VWR chemicals, 95 %). The $VOSO_4.n$H2O commercial powder was analysed by Inductively Coupled Plasma Optical Emission Spectroscopy (ICP-OES) to determine the number of water molecules (n) contained in the powder and the result showed that the powder was pentahydrate (n = 5). In Figure 1, the right storage tank ("sulfuric acid" side or negolyte) is initially filled with 2 M H_2SO_4 solution respectively. Note that the concentration of H_2SO_4 in the vanadium solution ("vanadium" side or posolyte) is not affected by the addition of $VOSO_4.nH_2O$ (this was determined by potentiometric titration, see below). The concentration of H_2SO_4 is initially the same on both sides (2 M).

Two peristaltic pumps (Cole Parmer, Masterflex® L/S® 07018-21) were used to circulate the solutions in two separate loops through the reactor at a constant flow rate of 40 L/h. The electrolytes volume is 200 mL.

As indicated in Figure 1, the experiments were conducted in two ways (case A and case B): first, experiments were carried out without polarization (I = 0, case A), this implies that no electrochemical reactions were taking place in the electrochemical cell. In this case, the storage tank, on the left that, initially containing the vanadium solution is named "vanadium" side, while the other one (on the right) is named "sulfuric acid" side. In the second case B,

experiments were conducted under galvanostatic polarization (I = 0.2 A). The left storage tank corresponds to the posolyte, while the right one corresponds to the negolyte. Throughout the experiment, the negolyte was continuously purged with humidified nitrogen to prevent the air oxidation of vanadium (II). Experiments are achieved at room temperature (18-22°C).

2.2. Analytical techniques

The volume variations in both compartments were monitored during experiments to evaluate the water transport across the Nafion^{TM} 424 membrane.

Samples of the electrolytes (1 mL) were undertaken at different times and the absorbance (A) values were measured at the three wavelengths: 855, 401 and 760 nm, respectively, for V^{2+}, V^{3+} and VO^{2+}, using a UV-vis spectrophotometer (Hewlett Packard Model 8453) and 1 cm thick quartz cuvettes. The Beer-Lambert's law (Eq. 1) was applied to calculate the corresponding concentration of V^{2+}, V^{3+} and VO^{2+} using respectively the extinction coefficient ε values: $\varepsilon_{855\,nm}$ = 2.04 L.mol^{-1}.cm^{-1}, $\varepsilon_{401\,nm}$ = 11.17 L.mol^{-1}.cm^{-1} and $\varepsilon_{760\,nm}$ = 19.92 L.mol^{-1}.cm^{-1}. These values were determined by El Hage [36] using vanadium solutions with different concentrations prepared in 3 M H_2SO_4.

$$A = -\log\frac{I_T}{I^\circ} = \varepsilon.l.c, \qquad (1)$$

where I_T and $I°$ are respectively the transmitted and the incident light intensities, l the thickness of the cuvette (1 cm) and c the concentration of the analyzed substance (mol.L^{-1}).

The potentiometric titration was used to determine the concentration of VO_2^+ and the acidity. The titration was carried out using an automatic potentiometric titration apparatus (888 Titrando Metrohm). The acidity corresponds here to the total amount of sulfuric acid H_2SO_4 and this gives access to the amount of "protons" available for self-discharge reactions, hydrogen evolution at the cathode and transported through the membrane. The titration, by

sodium hydroxide (Sigma Aldrich) 0.2 M, is performed as follows: 1 mL of the solution to titrate is diluted in 30 mL of ultrapure water in order to immerse the electrode. VO_2^+ and VO^{2+} do not interfere during dosage (on the dosing curves, VO^{2+} precipitates after the first dissociation of H_2SO_4 and no signal was observed for VO_2^+, this agrees with the result reported by El Hage [36]).

As for the titration of VO_2^+, 1 mL of the solution is also sampled and diluted in 30 mL of ultrapure water to immerse the electrode. The titrant solution used for the titration of VO_2^+ is Mohr's salt solution at 0.1 M, which is prepared by dissolving an amount of Mohr's salt (Sigma Aldrich, 99%) in ultra-pure water (18.2 MΩ.cm). Then, this solution was then acidified with H_2SO_4 at 3 M (BDH® VWR chemicals, 95%,) before the titration. A combined redox type electrode (Pt /…/ Cl^-/AgCl/ Ag) was used, and the titration reaction (I) involves two redox systems: VO_2^+/VO^{2+} and Fe^{3+}/Fe^{2+}.

$$VO_2^+ + 2H^+ + Fe^{2+} \rightarrow VO^{2+} + H_2O + Fe^{3+} \quad \text{(I)}$$

2.3. Deconvolution of UV-vis spectra of vanadium solutions

The UV-vis spectrum of a V^{2+} solution presents three peaks at 400, 600 and at 855 nm, while the spectrum of a V^{3+} solution exhibits two peaks at 401 and 610 nm. VO^{2+} in solution presents a peak at 760 nm. If the UV-vis technique is used for the analysis of an aqueous solution containing V^{2+}, V^{3+} and VO^{2+} species, the signal of V^{2+} at 855 nm can interfere with that of VO^{2+} at 760 nm, while the signals of V^{2+} and V^{3+} can overlap at two wavelengths around 400 and 600 nm. When peaks overlap in a UV-vis spectrum, a peak deconvolution method was applied, from a home-made python script, to extract/separate the signal of each vanadium ion. First, a baseline correction is applied to the raw UV-vis signal. The thus corrected UV-vis signal was then fitted by the sum of four Gaussian functions. A least mean squares process was

used and the initial conditions (guess) for the positions of the peaks were 400, 610, 760 and 855 nm. The amplitude and the position of the obtained peaks are used to analyse the temporal evolution of electrolyte composition.

3. Theoretical model

The composition of the solutions in the storage tanks is considered spatially uniform (well stirred tanks) and the corresponding concentration of each vanadium ion, c_v^i (or c_p^i) and c_s^i (or c_n^i) on the "vanadium" (or posolyte) and "sulfuric acid" (or negolyte) side, respectively, is referenced by the oxidation degree i which could be equal to II, III, IV and V for V^{2+}, V^{3+}, VO^{2+} and VO_2^+ respectively. The concentration of protons on the "vanadium" (or posolyte) and "sulfuric acid" (or negolyte) side is noted as $c_v^{H^+}$(or $c_p^{H^+}$) and $c_s^{H^+}$(or $c_n^{H^+}$), respectively. The volumes of electrolyte, at a given time, are given by $V_v(t)$ (or $V_p(t)$) and $V_s(t)$ (or $V_n(t)$) for the "vanadium" (or posolyte) and "sulfuric acid" (or negolyte) side, respectively.

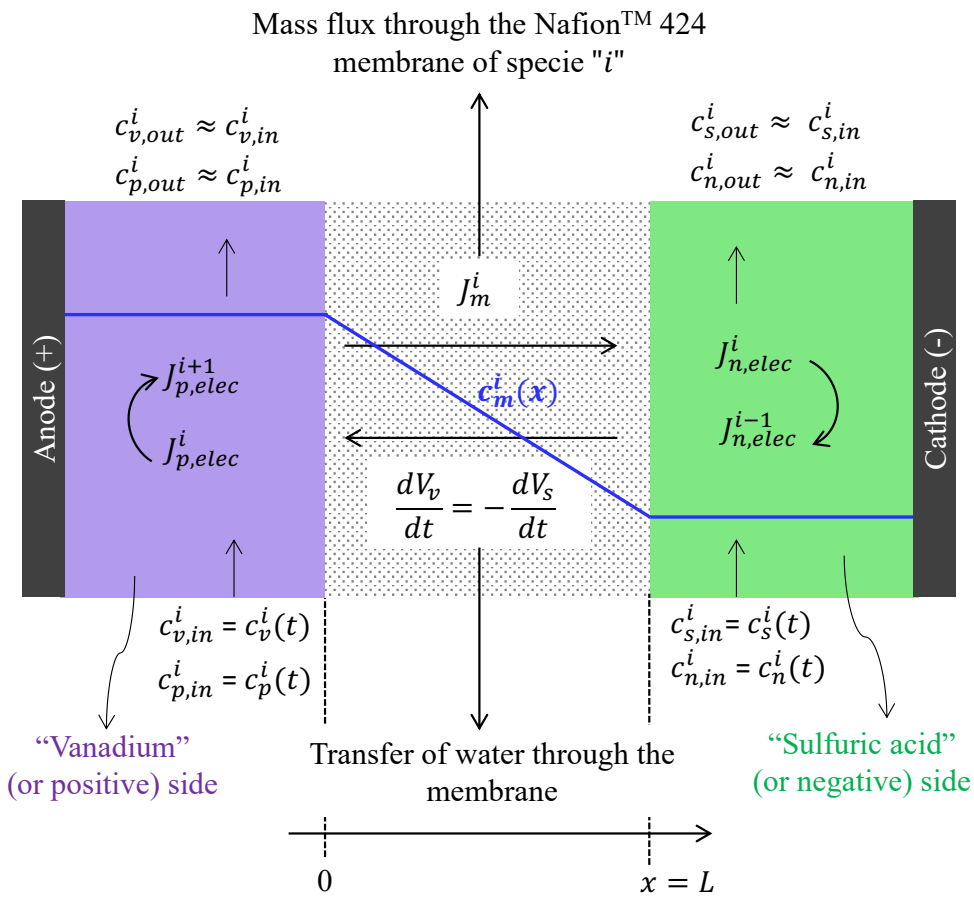

Figure 3: Sketch of the electrochemical reactor and of the considered fluxes between the two compartments through the membrane.

During one residence time into the electrochemical reactor, the conversion is considered low in such a way that the outlet concentrations, $c^i_{v,out}$ (or $c^i_{p,out}$) and $c^i_{s,out}$ (or $c^i_{n,out}$) for vanadium (or posolyte) and sulfuric acid (or negolyte) sides respectively, are close to the inlet concentrations $c^i_{v,in}$ (or $c^i_{p,in}$) and $c^i_{s,in}$ (or $c^i_{n,in}$), as sketched in Figure 3. Consequently, the concentrations in the electrochemical reactor can be considered as equal to $c^i_v(t)$ (or $c^i_p(t)$) and $c^i_s(t)$ (or $c^i_n(t)$) for the vanadium (or posolyte) and sulfuric acid (or negolyte) side respectively. Moreover, the outlet solutions are immediately diluted into the storage tanks, thus the overall conversion of the electroactive species into the whole electrolytes remains low anyway.

Here, what is interesting to monitor, are the concentrations into the storage tanks, $c_v^i(t)$ (or $c_p^i(t)$) and $c_s^i(t)$ (or $c_n^i(t)$). The water volumetric flux through the membrane is given by dV_v/dt = - dV_s/dt, where V_v and V_s are the volumes of the "vanadium" and "sulfuric acid" sides, respectively, in case A (without polarization), and by dV_p/dt = - dV_n/dt, where V_p and V_n are the volumes of the posolyte and negolyte, respectively, in case B (with polarization).

3.1. Model for experiment without polarization (case A)

In the absence of an applied electric current, no electrochemical and self-discharge reactions are expected. However, the VO^{2+} ions ($i = IV$) diffuse through the membrane from vanadium towards sulfuric acid side. The concentration profile of VO^{2+} into the membrane, $c^{IV}(x)$, is assumed as linear as sketched in Figure 3 (steady state diffusion). The diffusion flux of VO^{2+} through the membrane $J_{D_m}^{IV}$ is given by the Fick's first law [12,13,23]:

$$J_{D_m}^{IV} = -S_m . D_m^{IV} . \frac{\partial C_m^{IV}}{\partial x} = -S_m . D_m^{IV} . \frac{(C_s^{IV} - C_v^{IV})}{L}, \quad (2)$$

where D_m^{IV} is the effective diffusion of VO^{2+} ions through the Nafion™ 424 membrane, S_m the surface area of the membrane (equal to the useful surface area of the electrodes i.e., 20 cm^2) and L the thickness of the membrane (200 µm). The mass balance of VO^{2+} ions in the storage tank on the vanadium side leads to:

$$\frac{d(C_v^{IV} . V_v)}{dt} = -J_{D_m}^{IV}. \quad (3)$$

By taking into account the variation of the volume, the latter equation becomes:

$$\frac{dC_v^{IV}}{dt} = \frac{1}{V_v}\left[-J_{D_m}^{IV} - c_v^{IV}\frac{dV_v}{dt}\right]. \quad (4)$$

The same analysis can be performed on the sulfuric acid side:

$$\frac{dC_s^{IV}}{dt} = \frac{1}{V_s}\left[J_{D_m}^{IV} - C_s^{IV}\frac{dV_s}{dt}\right]. \quad (5)$$

Concerning H^+ concentration, the same approach can be used and the corresponding mass balance on the "vanadium" side is given as follows:

$$\frac{dC_v^{H^+}}{dt} = \frac{1}{V_v}\left[-J_{D_m}^{H^+} - c_v^{H^+}\frac{dV_v}{dt}\right], \quad (6)$$

$$J_{D_m}^{H^+} = -S_m . D_m^{H^+}\frac{\partial C_m^{H^+}}{\partial x} = -S_m . D_m^{H^+} . \frac{\left(c_s^{H^+} - c_v^{H^+}\right)}{L}, \quad (7)$$

where $c_v^{H^+}$ and $c_s^{H^+}$ are the proton concentration in the storage tank on the vanadium and sulfuric acid sides respectively, $D_m^{H^+}$ the diffusion coefficient of protons in the membrane and $c_m^{H^+}(x)$ the proton concentration in the membrane (Figure 3). However, here the difference in H^+ concentration across the membrane ($c_v^{H^+} - c_s^{H^+}$) remains low (contrary to that of the vanadium $c_v^{IV} - c_s^{IV}$) and the diffusion flux of H^+ can be safely neglected compared to the flux term related to volume variation of storage tanks. Under this condition, the mass balances of H^+ on the vanadium and sulfuric acid sides are given by Eq. 8 and 9, respectively, as follows:

$$\frac{dC_v^{H^+}}{dt} = \frac{1}{V_v}\left[-c_v^{H^+}\frac{dV_v}{dt}\right], \quad (8)$$

$$\frac{dC_s^{H^+}}{dt} = \frac{1}{V_s}\left[-c_s^{H^+}\frac{dV_s}{dt}\right]. \quad (9)$$

Eq. 4-5 and 8-9 are ordinary differential equations and they are solved numerically using the python function scipy.integrate.odeint. Second order polynomial functions are used to model V_v and V_s. These later functions are adjusted with the experimentally measured temporal variations of the electrolyte volumes.

3.2. Model for experiment under galvanostatic polarization (case B)

Figure 4 illustrates in detail the expected composition variations in the reactor operating under galvanostatic polarization. It is indicated that the concentration of the different species in respective storage tanks is affected not only by the crossover mechanism between the two half-cells but also by electrochemical and self-discharge reactions occurring on each side as described in reactions Rx. II-IX (electrochemical reactions) and Rx. X-XII (for self-discharge reactions).

On the positive side, the VO^{2+} ions are expected to be converted to VO_2^+ by electrochemical oxidation reaction (Rx. II). Moreover, gradients in electric potential and concentration between the positive and the negative side can lead to the transfer of VO^{2+} and VO_2^+ across the membrane towards the negative side (crossover). In the negative side, the transported ions, VO_2^+ and VO^{2+}, may be electrochemically reduced into various intermediate species (VO^{2+}, V^{3+}, etc) and ultimately leading to V^{2+} (Rx. VI to VIII). V^{3+} and V^{2+} ions can diffuse across the membrane towards the positive side and be oxidized at the electrode to finally led to VO_2^+ (Rx. III and IV).

Concerning the protons, they are produced on the positive side by electrochemical oxidation of both VO^{2+} (Rx. II), V^{3+} (Rx III) and V^{2+} (Rx. IV), to V(V), involving, respectively, 2, 4 and 4 mol of H^+ produced per mol of V(V). The oxidation of the solvent, H_2O, may occur resulting in H^+ production (Rx. V). Furthermore, migration of H^+ ions across the membrane (from positive to negative side) will occur to balance the charges. On the negative side, H^+ are consumed by direct electrochemical reduction (Rx. VI) and by electrochemical reduction of VO^{2+} and VO_2^+ (Rx. VII and VIII). Furthermore, the self-discharge reactions, which are considered irreversible, may occur in both sides, as a result of vanadium species crossover [28],

as described by reactions Rx. X to XII, leading to the production (or consumption) of vanadium species and the consumption of H^+ species.

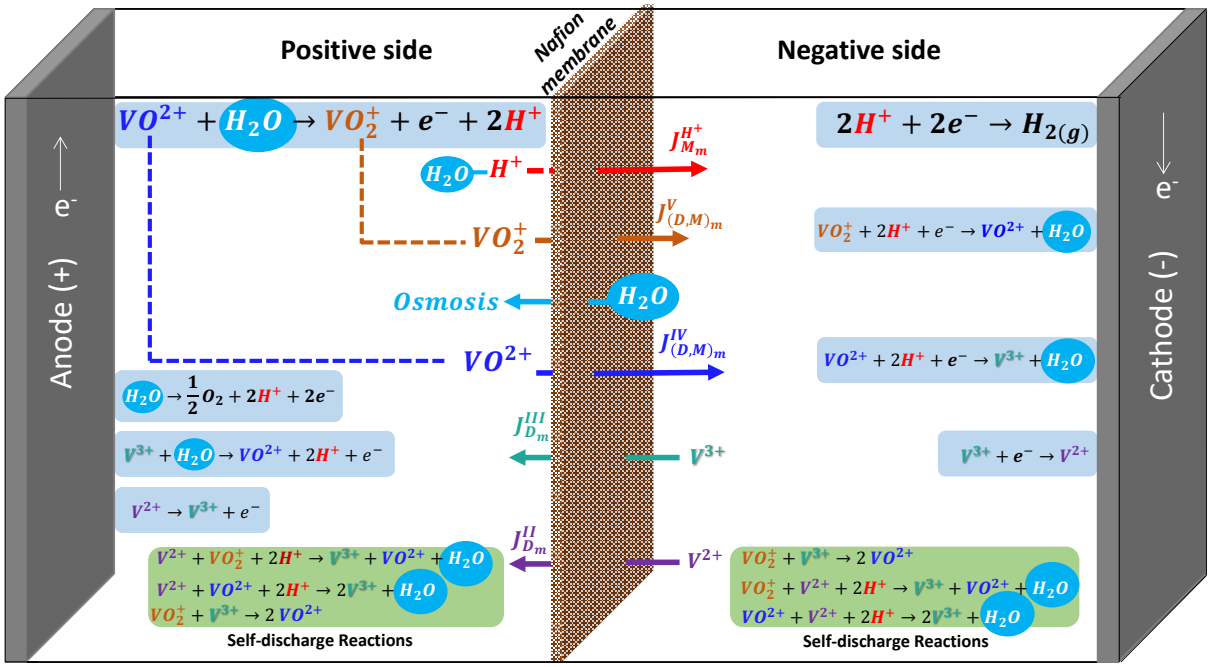

Figure 4: Model domain of experiment operating under galvanostatic polarization (electrochemical and self-discharge reactions are represented on a blue and green background respectively, $J^i_{D_m}$ is the diffusion (D) flux of specie "i" across membrane and $J^i_{(D,M)_m}$ the diffusion (D) and migration (M) flux of specie "i" across membrane).

However, due to the fact that the expected concentrations of VO^{2+} and VO_2^+ in negolyte (c_n^{IV} and c_n^{V}), and of V^{2+} and V^{3+} in posolyte (c_p^{II} and c_p^{III}), may remain as low as one hundredth of the concentration of H^+ (~2 M), the H^+ consumed by the electrochemical reductions of VO^{2+} and VO_2^+ in negolyte, or by electrochemical oxidation of V^{2+} and V^{3+} in posolyte, can be considered as negligible. This also results in a negligible effect of self-discharge reactions on the concentration of H^+.

On the positive side, the expected electrochemical reactions are:

$$VO^{2+} + H_2O \rightarrow VO_2^+ + e^- + 2H^+, \qquad \text{(II)}$$

$V^{3+}+H_2O \rightarrow VO^{2+}+2H^{+}+e^{-}$, (III)

$V^{2+} \rightarrow V^{3+} + e^{-}$, (IV)

$H_2O \rightarrow \frac{1}{2}O_{2(g)} + 2e^{-} + 2H^{+}$. (V)

On the negative side, the expected electrochemical reactions are:

$2H^{+} + 2e^{-} \rightarrow H_{2(g)}$, (VI)

$VO_2^{+} + 2H^{+} + e^{-} \rightarrow VO^{2+} + H_2O$, (VII)

$VO^{2+} + 2H^{+} + e^{-} \rightarrow V^{3+} + H_2O$, (VIII)

$V^{3+} + e^{-} \rightarrow V^{2+}$. (IX)

The self-discharge reactions on the posolyte and negolyte sides are:

$V^{3+} + VO_2^{+} \xrightarrow{k^{III,V}} 2VO^{2+}$, (X)

$VO_2^{+} + V^{2+} + 2H^{+} \xrightarrow{k^{II,V}} V^{3+} + VO^{2+} + H_2O$, (XI)

$V^{2+} + VO^{2+} + 2H^{+} \xrightarrow{k^{II,IV}} 2V^{3+} + H_2O$, (XII)

where $k^{i,j}$ refers to the rate constant of a self-discharge reaction involving vanadium species with the oxidation degree *i* and *j*.

Taking into account the above considerations, the global mass balance equations for a vanadium specie *i* is given in Eq. 10 and 11 on posolyte and negolyte sides, respectively:

$$\frac{dc_p^i}{dt} = \frac{1}{V_p}\left[-J^i_{(D,M)_m} + J^i_{p,elec} + \alpha^i - c_p^i \frac{dV_p}{dt}\right], \quad (10)$$

$$\frac{dc_n^i}{dt} = \frac{1}{V_n}\left[J_{(D,M)_m}^i + J_{n,elec}^i + \alpha^i - c_n^i \frac{dV_n}{dt}\right], \quad (11)$$

where $J_{(D,M)_m}^i$ is the overall (diffusion and migration) mass flux of vanadium specie with an oxidation degree i across Nafion™ 424 membrane, $J_{p,elec}^i$ and $J_{n,elec}^i$ correspond to the net mass flux (production – consumption) of vanadium specie with an oxidation degree i caused by the electrochemical reactions on the positive and negative sides respectively and α^i is the net mass flux of vanadium specie with an oxidation degree i caused by self-discharge reactions.

Concerning the protons, the corresponding mass balance equation in posolyte and negolyte are given in Eq. 12 and 13, respectively, as follows:

$$\frac{dc_p^{H^+}}{dt} = \frac{1}{V_p}\left[-J_{M_m}^{H^+} + J_{p,elec}^{H^+} - c_p^{H^+} \frac{dV_p}{dt}\right], \quad (12)$$

$$\frac{dc_n^{H^+}}{dt} = \frac{1}{V_n}\left[J_{M_m}^{H^+} + J_{n,elec}^{H^+} - c_n^{H^+} \frac{dV_n}{dt}\right], \quad (13)$$

where $J_{M_m}^{H^+}$ is the mass flux of H^+ through the membrane, $J_{p,elec}^{H^+}$ and $J_{n,elec}^{H^+}$ are the net mass flux (production – consumption) of H^+ caused by the electrochemical reactions on the positive and negative sides respectively. Second order polynomial functions are used to fit the electrolyte volume variation in the two storage tanks, thus providing terms that best describes the volume change of specific storage tank, as mentioned where experiment is conducted without polarization.

- *Determination of the mass fluxes:* $J_{(D,M)_m}^i$ and $J_{M_m}^{H^+}$

The mass flux of vanadium specie i across the membrane, $J_{(D,M)_m}^i$, is given by the sum of diffusion and migration fluxes as follows:

$$J^i_{(D,M)_m} = \underbrace{-D^i_m S_m \frac{dc^i_m}{dx}}_{J^i_{D_m}} + \underbrace{z^i F u^i_m S_m c^i_m E}_{J^i_{M_m}}, \quad (14)$$

where F is the Faraday constant, E the electric field, z^i the valence, u^i_m the effective mobility and c^i the local concentration in the membrane (at a given location on the *x*-axis, Figure 3) of a vanadium ion with an oxidation degree i.

Due to the electric field, the concentration profile in the membrane is no longer linear (Eq. 14). The concentration profile can be determined by solving the transport problem in the membrane by considering that the transport by diffusion and migration in the membrane is at the steady-state ($J^i_{(D,M)_m}$ = constant along *x*-axis). The derivation of Eq. 14, assuming E constant in the membrane, leads to:

$$-D^i_m \frac{d^2c^i}{dx^2} + z^i F u^i_m E \frac{dc^i}{dx} = 0. \quad (15)$$

The corresponding boundary conditions associated to the Eq. 15 are:

$$\begin{cases} c^i_m(x = 0) = c^i_p(t) \\ c^i_m(x = L) = c^i_n(t) \end{cases} \quad (16)$$

The Eq. 15 and the associated boundary conditions (Eq. 16) correspond to a boundary value problem which is numerically solved with the python function scipy.integrate.solve_bvp. $J^i_{(D,M)_m}$ is computed for each pair of values ($c^i_p(t)$ and $c^i_n(t)$), from the obtained values of $c^i(x)$, and by using Eq. 14.

From the Nernst-Einstein equation, we assume that the effective mobility u^i_m is related to the effective diffusion coefficient in the membrane as follows:

$$u^i_m = \frac{D^i_m}{RT}, \quad (17)$$

where R is the ideal gas constant and T the temperature.

In the Eq. 15, E is considered as spatially constant in the membrane and expressed as:

$$E = \frac{\Delta V_m}{L} = \frac{I R_m}{L} = \frac{I}{\sigma_m S_m}, \quad (18)$$

where ΔV_m is the voltage drop across the membrane, R_m the electric resistance and σ_m the ionic conductivity of the membrane. Note that assuming E constant implies that σ_m is also assumed constant and thus not dependent on the local concentration of vanadium ions $c^i(x)$; this appears reasonable since the conductivity of the membrane is expected to be more dependent on proton concentration and for the investigated situations proton concentration difference across membrane remains low.

As aforementioned, the mass flux of H^+ across membrane corresponds meanly to the migration flux of H^+ towards negative side to balance charges. The migration flux of H^+ is expressed as a function of the transference number of H^+ across the Nafion™ 424 membrane, t^{H^+}, for which a value of 0.97 was used (according to the supplier).

$$J_{M_m}^{H^+} = \frac{t^{H^+} I}{F}, \quad (19)$$

where I is the applied current (A).

- *Determination of the electrochemical net mass fluxes:* $J_{p\ (or\ n),elec}^{i}$ and $J_{p\ (or\ n),elec}^{H^+}$

The electrochemical net mass flux of a specie i expresses the difference between the amount specie produced and consumed by electrochemical reactions. The amount of specie (produced or consumed) lies mainly to the electrochemical kinetic rate, which is a function of the current, I, available. Since experiments are carried out under galvanostatic mode, the partitioning of the applied current, I, between all possible electrochemical reactions, on both sides and at any time,

can be determined by comparing the limiting currents for each vanadium ions, I_{lim}^{i}, to the applied current I. More precisely, this is performed using logical tests by comparing the sum of the limiting currents to the applied current. The limiting current of a specie i is given as follows:

$$I_{lim}^{i} = SFk_{c}^{i}c^{i}, \tag{20}$$

where S is the electrode surface area, k_{c}^{i} is the mass transfer coefficient and c^{i} the concentration of vanadium ion with the oxidation degree i on positive side (c_{p}^{i}) or on negative side (c_{n}^{i}).

Concerning the posolyte side, Figure 5(a) illustrates a schematic theoretical current-potential curve that could be obtained by electrochemically oxidizing a solution of vanadium (II) (containing or not all the four forms of vanadium ions), assuming a fast electrochemical reaction for all vanadium species. Three successive oxidations of vanadium ions could occur before the oxidation of the solvent H_2O at higher potentials. This chart can be used to determine the partitioning of the applied current I during a galvanostatic electrolysis. To do this, three sums of limiting currents are defined:

$$I_{lim,p(II,III,IV)} = \sum_{i=II}^{i=IV} I_{lim}^{i}, \tag{21}$$

$$I_{lim,p(II,III)} = \sum_{i=II}^{i=III} I_{lim}^{i}, \tag{22}$$

$$I_{lim,p(II)} = I_{lim}^{II}. \tag{23}$$

Based on this figure (Figure 5a), the corresponding algorithm includes four cases described as follows:

- case 1: $I_{lim,p(II,III,IV)} < I$, which implies that a part of the current is used to oxidize water. The consumption flux of each vanadium ions is then given by $k_c^i Sc_p^i$, the consumption of vanadium species is limited by mass transfer, Figure 5(b).
- case 2: $I_{lim,p(II)} > I$, the consumption flux of V^{2+} is lower than its maximum value $k_c^{II} Sc_p^{II}$, it is fixed by the applied current and equal to I/F, Figure 5(c).
- case 3: $I_{lim,p(II,III)} > I > I_{lim,p(II)}$, full consumption of V^{2+} at the electrode interface, consumption flux of $V^{2+} = k_c^{II} Sc_p^{II}$, partial consumption of V^{3+}, consumption flux of $V^{3+} = \frac{I}{F} - k_c^{II} Sc_p^{II}$, Figure 5(d).
- case 4: $I_{lim,p(II,III,IV)} > I > I_{lim,p(II,III)}$, full consumption of V^{2+} (consumption flux of $V^{2+} = k_c^{II} Sc_p^{II}$), full consumption of V^{3+} (consumption flux of $V^{3+} = k_c^{III} Sc_p^{III}$) and partial consumption of VO^{2+} (consumption flux of $VO^{2+} = \frac{I}{F} - k_c^{II} Sc_p^{II} - k_c^{III} Sc_p^{III}$), Figure 5(e).

Using the consumption fluxes above-determined, the electrochemical production fluxes can be deduced from the rule: (production flux of vanadium specie i) = (consumption flux of vanadium specie i – 1). The net mass flux of each vanadium ions in positive side, $J_{p,elec}^i$, is given as follows:

$$J_{p,elec}^i = \text{(production of } i\text{)} - \text{(consumption of } i\text{)}. \quad (24)$$

Note that there is no electrochemical consumption of VO_2^+ (consumption of $VO_2^+ = 0$) and no electrochemical production of V^{2+} (production of $VO_2^+ = 0$) on posolyte side.

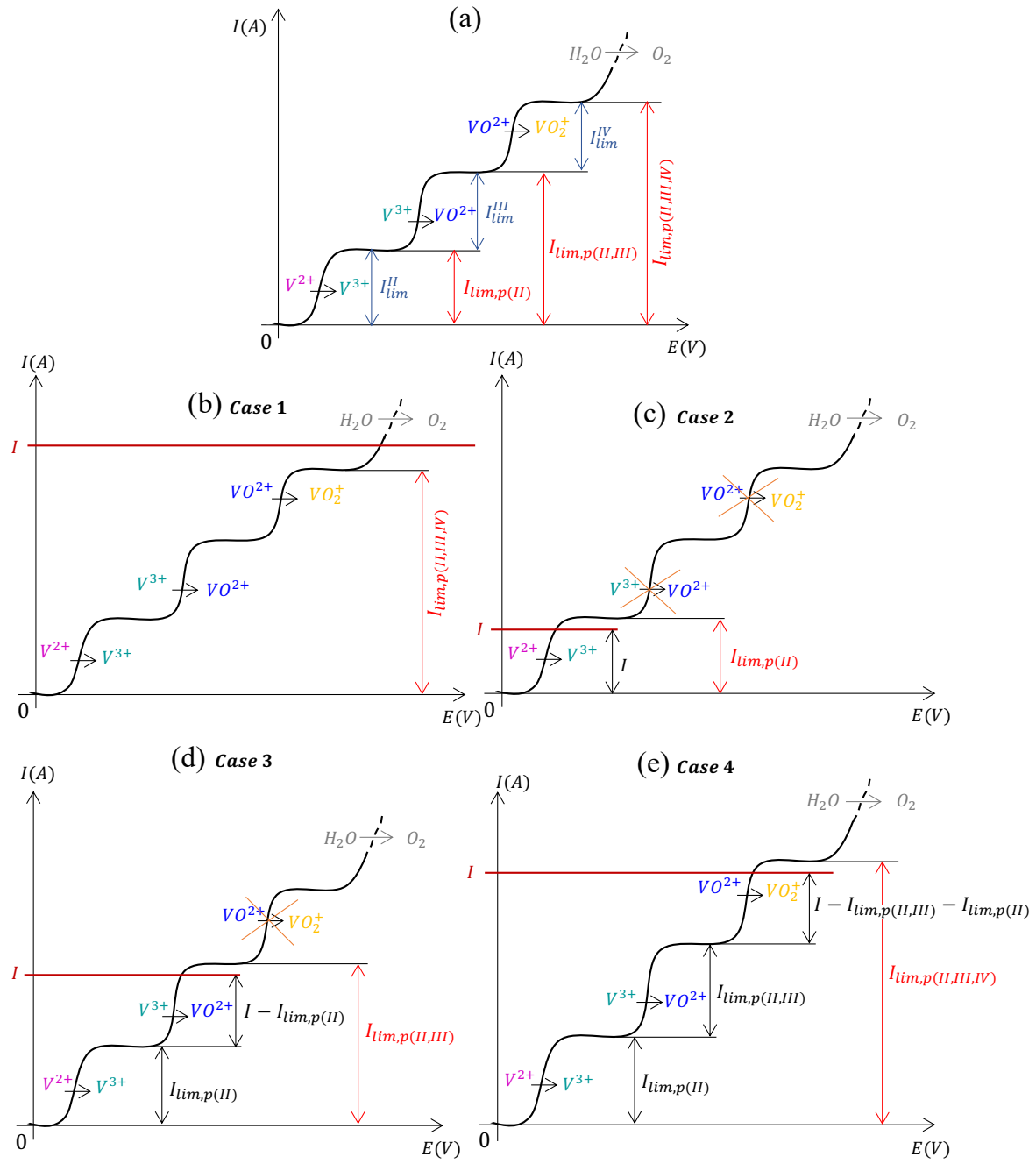

Figure 5: Representation of the current-potential curve expected when applying positive currents (oxidation) to a stirred solution containing the four forms of vanadium ions (a). Illustrations of the partitioning of current on positive side for the case 1 (b), 2 (c), 3 (d) and 4 (e).

On the negolyte side, the same process is used to determine net mass flux, $J^i_{p,elec}$, of each vanadium specie. The partitioning of the current is performed using also three limiting currents defined as follows:

$$I_{lim,n(III,IV,V)} = \sum_{i=III}^{i=V} I^i_{lim} \quad (25)$$

$$I_{lim,n(IV,V)} = \sum_{i=IV}^{i=V} I^i_{lim} \quad (26)$$

$$I_{lim,n(V)} = I^V_{lim}. \quad (27)$$

The corresponding algorithm for the negolyte side is provided below including four cases as follows:

- case 1: $I_{lim,n(III,IV,V)} < I$ and therefore a part of the current is used for hydrogen gas production. The consumption flux of each vanadium ions is then given by $-k^i_c Sc^i_n$
- case 2: $I_{lim,n(V)} > I$, partial consumption of VO_2^+ and the consumption flux is fixed by the applied current and equal to $-I/F$. No electrochemical consumption of VO^{2+}
- case 3: $I_{lim,n(IV,V)} > I > I_{lim,n(V)}$, full consumption of VO_2^+ and the corresponding consumption flux is $-k^V_c Sc^V_n$. Partial consumption of VO^{2+} and the corresponding consumption flux is $-(\frac{I}{F} - k^V_c Sc^V_n)$
- case 4: $I_{lim,n(III,IV,V)} > I > I_{lim,n(IV,V)}$, full consumption of VO_2^+ (consumption flux of $VO_2^+ = -k^V_c Sc^V_l$), full consumption of VO^{2+} (consumption flux of $VO^{2+} = -k^{IV}_c Sc^{IV}_n$), partial consumption of V^{3+} (consumption flux of $V^{3+} = -(\frac{I}{F} - k^V_c Sc^V_n - k^{IV}_c Sc^{IV}_n)$).

As for the posolyte (Eq. 24), the net mass flux of each vanadium ion on the negative side, $J^i_{n,elec}$, is given by:

$$J^i_{n,elec} = (\text{production of } i) - (\text{consumption of } i). \quad (28)$$

Note that, it is assumed that no electrochemical consumption of V^{2+} (consumption flux of V^{2+} = 0) and no electrochemical production of VO_2^+ (production flux of VO_2^+ = 0) occur on the negative side. Concerning the electrochemical production of V^{2+}, V^{3+} and VO^{2+}, it is assumed that V^{2+}, V^{3+} and VO^{2+} are produced by electrochemical reduction of V^{3+}, VO^{2+} and VO_2^+, respectively, the final product being V^{2+}.

Following this process, $J_{p,elec}^{i}$ and $J_{n,elec}^{i}$ are determined at each time step from the values of $c_p^i(t)$ and $c_n^i(t)$. The values of the mass transfer coefficients k_c^i are taken from the work of El Hage [36] who studied mass transfer of each vanadium specie using the same reactor as in this study.

As for protons on the positive side, $J_{p,elec}^{H^+}$ is determined following the same approach as for vanadium species on the posolyte side. The corresponding algorithm is presented below including four cases:

- case 1: $I > I_{lim,p(II,III,IV)}$, production of H^+ by electrochemical oxidation of H_2O (production flux of H^+ = $\left[\frac{I-I_{lim,p(II,III,IV)}}{F}\right]$ and by full oxidation of VO^{2+} and V^{3+} (production flux of $H^+ = 2k_c^{IV}Sc_p^{IV} + 2k_c^{III}Sc_p^{III}$)
- case 2: $I < I_{lim,p(II)}$, production flux of H^+ = 0 (only oxidation of V^{2+} occurs)
- case 3: $I_{lim,p(II)} < I < I_{lim,p(II,III)}$, oxidation of V^{2+} and V^{3+} occurs and the corresponding H^+ production flux is $2\left[\left(\frac{I}{F}\right) - k_c^{II}Sc_p^{II}\right]$)
- case 4: $I_{lim,p(II,III)} < I < I_{lim,p(II,III,IV)}$, full oxidation of V^{3+} (production flux = $2k_c^{III}Sc_p^{III}$) and partial oxidation of VO^{2+} (production flux = $2\left[\left(\frac{I}{F}\right) - -k_c^{II}Sc_p^{II} - k_c^{III}Sc_p^{III}\right]$.

On the negolyte side, H^+ is mainly consumed by direct electrochemical reduction as aforementioned. Consequently, the net mass flux of H^+ in negative side, $J_{n,elec}^{H^+}$, is expressed as:

$$J_{r,elec}^{H^+} = -I/F \tag{29}$$

- *Determination of net mass flux due to the self-discharge reactions:* α^i

Based on the reactions Rx. X to XII, the net mass flux of different vanadium ions caused the self-discharge reactions are given by:

$$\alpha^{II} = -r_{II,IV} - r_{II,V} \tag{30}$$

$$\alpha^{III} = -r_{III,V} + 2r_{II,IV} + r_{II,V} \tag{31}$$

$$\alpha^{IV} = 2r_{III,V} - r_{II,IV} + r_{II,V} \tag{32}$$

$$\alpha^{V} = -r_{III,V} - r_{II,V} \tag{33}$$

Where α^i is the net mass flux of vanadium specie with an oxidation degree i caused by self-discharge reactions and $r^{i,j}$ the reaction rate of a self-discharge reaction involving vanadium species with the oxidation degree i and j.

The reaction rate of the self-discharge reactions, $r_{i,j}$, can be written as a function of self-discharge reaction rate constant, $k^{i,j}$, and concentration of vanadium ions involved in the reaction raised to the corresponding reaction orders n_i and n_j as follows:

$$r^{i,j} = k^{i,j}\left(T, c^{H^+}\right) \times (c^i)^{n_i}(c^j)^{n_j} \times V_{p/n}. \tag{34}$$

In this study, we consider, $n_i = n_j = 1$ (this corresponds to the stoichiometry of the reactions assuming simple chemical mechanisms). Moreover, the self-discharge reactions are assumed instantaneous on both sides as reported by Tang et al. [28]. Thus, a sufficiently high value of $k^{i,j}$ is used for the numerical resolution of the problem (so that the solution does not depend on $k^{i,j}$).

4. Results and discussion

4.1. Experiment without polarization (case A)

Starting from the "vanadium" side containing 1.7 M VO^{2+} in 2 M sulfuric acid and the "sulfuric acid" side containing only 2M sulfuric acid, the parameters of interest (electrolyte volumes, VO^{2+} concentration and acid concentration) are measured as a function of time.

Figure 6 shows the volume change of the electrolytes on both sides after 50 h. The electrolyte volume increased on the "vanadium" side and decreased on the "sulfuric acid" side during experiment, indicating that the transport direction of water is towards "vanadium" side. Water transport, in absence of an electric field, is mainly driven by vanadium crossover with bound water and by osmosis. In the first case, water transport is expected to occur from "vanadium" to "sulfuric acid" side and the volume of the transported water depends on the amount of VO^{2+} transported by diffusion. In contrast, the water transport induced by osmosis will be in opposite direction, since "vanadium" side contains more ionic species and therefore has a higher osmosis pressure than the other side. Since diffusion is expected to occur from "vanadium" to "sulfuric acid" side, the water transported by crossover of VO^{2+} would be in the same direction, expecting an increase in electrolyte volume in "sulfuric acid" storage tank. By considering the curves in Figure 6, it can be concluded that osmosis is the prevailing transport mechanism controlling water transport across Nafion™ 424 membrane in case A. Furthermore, the amount of VO^{2+} that diffused towards "sulfuric acid" storage tank after 50 h is equal to

0.0038 mol (from data shown in Figure 6) which is very low and subsequently the volume of the corresponding water transported can be considered negligible.

The average specific water flux, $J_{D_m}^{W}$, estimated using temporal electrolyte volume variation on "sulfuric acid" side, is equal to 0.42 $L.m^{-2}.h^{-1}$ (i.e., 2.1 mL/cm^2 during 50 h). This value is high compared to e.g. that reported by Zeng et al., for a raw or modified Nafion 117 membrane (0.72 mL/cm^2 during 72h and 0.22 mL/cm^2 during 72h for raw and modified membrane respectively) [37]. However, the high value obtained in the present work can be explained by the high difference in initial vanadium concentration between the two sides, corresponding to an osmotic pressure of ~40 bar (from van't Hoof law, osmotic pressure = (concentration difference = 1.7 M)× RT). The corresponding osmotic pressure in the work of Zeng et al. is expected to be much smaller because they used two solutions initially charged at 50% of SoC (posolyte 1.5M VO_2^+/VO^{2+} and negolyte 1.5M V^{3+}/V^{2+}).

It is observed that the volume decrease on "sulfuric acid" side (200 - 158 = 42 mL, 21%) is slightly higher than the increase on "vanadium" side (237 - 200 = 37 mL, 18.5%), the corresponding relative gap is 13% (21/18.5-1). This can be attributed to water evaporation faster in the vanadium tank than in the sulfuric acid tank because of the higher level of solution (the tanks have the same dimensions) and this results in a lower apparent variation in volume on the vanadium side. On the sulfuric acid side, the solvation of vanadium ions by the water consumes the water and causes a higher apparent variation in volume.

Each temporal evolution of electrolyte volume (V_v(t) and $V_s(t)$) is fitted by a second order polynomial function. The thus fitted curves coincide well with experiment data, Figure 6.

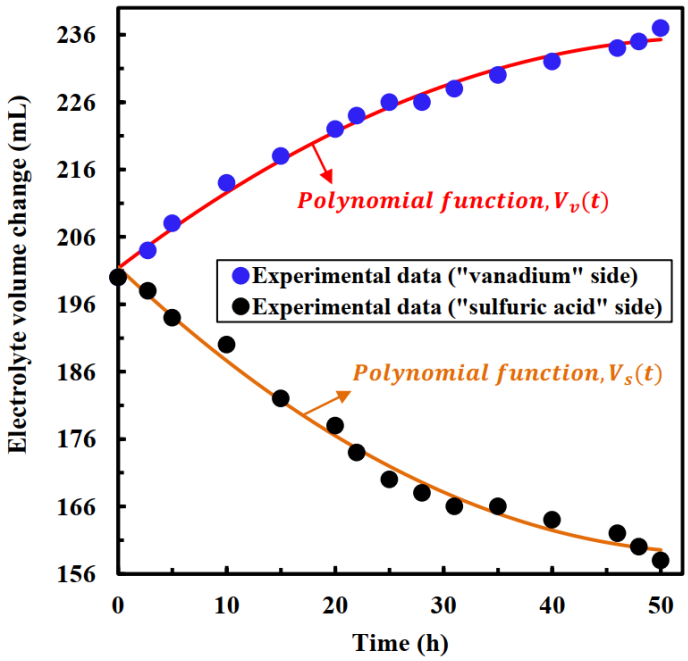

Figure 6: Temporal evolution of the electrolyte volume on the "vanadium" (blue disks) and "sulfuric acid" (black disks) side (see Figure 1) and the corresponding second order polynomial fit curves (flowrate = 40 L.h^{-1}, initial conditions on "Vanadium" side: $V_v(0)$ = 200 mL, [H_2SO_4] = 2.05 mol.L^{-1}, [VO^{2+}] = 1.69 mol.L^{-1} and on "sulfuric acid" side: $V_s(0)$ = 200 mL, [H_2SO_4] = 2.02 mol.L^{-1}).

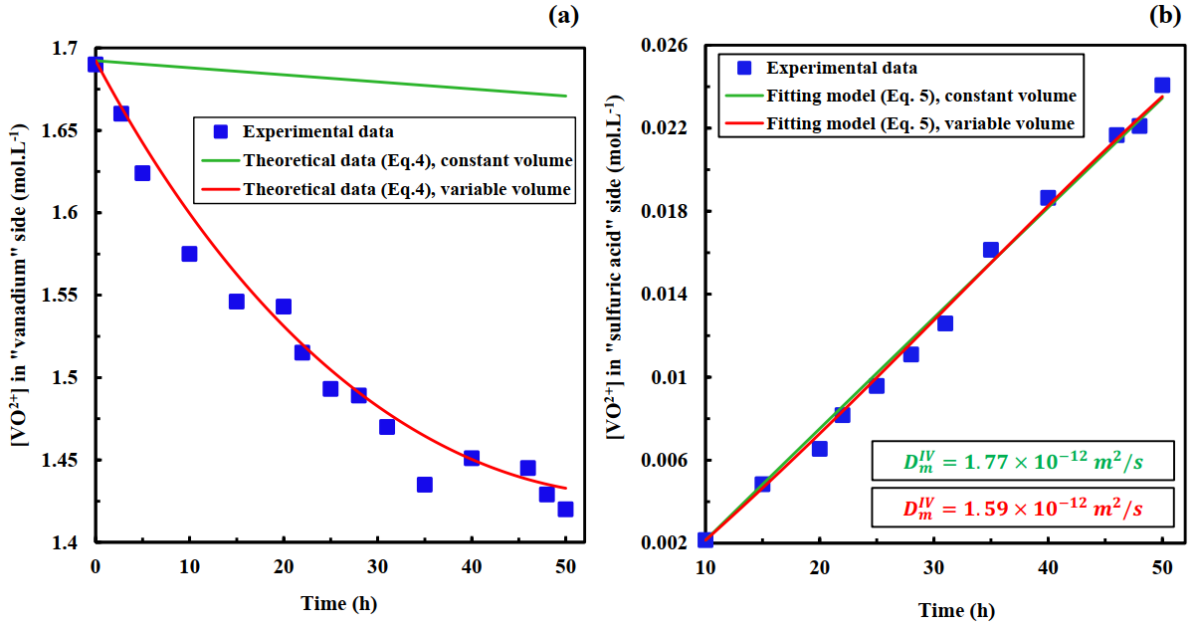

Figure 7: Experimental (blue squares) and theoretical (red and green lines) temporal evolutions of VO^{2+} concentration on "vanadium" (a) and "sulfuric acid" (b) side. The values of the effective diffusion coefficient of VO^{2+}, D_m^{IV}, 1.77×10^{-12} m^2/s and 1.59×10^{-12} m^2/s, are obtained by fitting experiment data of "sulfuric acid" side, see the text (b); the numerical resolution of Eq. 5 is performed in two ways: constant and variable electrolyte volume; flowrate = 40 L.h^{-1}, initial conditions on "Vanadium" side: $V_v(0)$ = 200 mL, [H_2SO_4] = 2.05 mol.L^{-1}, [VO^{2+}] = 1.69 mol.L^{-1} and on "sulfuric acid" side: $V_s(0)$ = 200 mL, [H_2SO_4] = 2.02 mol.L^{-1}.

Figure 7(a) and 7(b) show the experimental and theoretical temporal evolution of VO^{2+} concentration on "vanadium" and "sulfuric acid" sides respectively.

Figure 7 (b) indicates that VO^{2+} specie appears and is enriched over time, which is the result of diffusion across the membrane. The effective diffusion coefficient of VO^{2+} across the Nafion™ 424 membrane D_m^{IV} is determined by fitting the theoretical temporal evolution of VO^{2+} concentration on "sulfuric acid" side, $c_s^{IV}(t)$, obtained by numerical integration of Eq. 5, with experiment data, Figure 7(b).

The numerical resolution of Eq. 5 is performed in two ways: by considering the electrolyte volume V_s as constant and as variable over time (using the fitted polynomial function in Figure 6). This comparison is conducted to evaluate the effect of variation in electrolyte volume on the estimation of concentration and effective diffusion coefficient values.

The fitting process is performed starting from 10h, which corresponds to the time at which the first concentration of VO^{2+} (c_s^{IV}) was detected (quantitively measurable) on the "sulfuric acid" side. The obtained D_m^{IV} when the electrolyte volume is considered as constant (D_m^{IV} = 1.77× 10^{-12} $m^2.s^{-1}$) is higher of about 11% than that when the variation in electrolyte volume is taken into account (D_m^{IV} = 1.59 × 10^{-12} $m^2.s^{-1}$). However, the fitting curves for the two cases (red and green lines), displayed in Figure 7(b), exhibit approximately the same trend without significant difference and match well with experimental data. The corresponding coefficients of determination (R^2) for the two considered cases are equal to 0.9985 (constant electrolyte volume) and 0.9990 (variable electrolyte volume), which are approximately the same. The obtained values of D_m^{IV} are of the same order of magnitude as the values previously reported in the bibliography using other Nafion membranes (especially N117) [16,37,38].

On the "vanadium" side, the experimentally measured VO^{2+} concentration decreased approximately by 16% after 50 h, Figure 7(a). The theoretical prediction of the temporal

evolution of VO^{2+} concentration, $c_v^{IV}(t)$, is determined by the numerical integration of Eq. 4, for the two considered cases: constant or variable electrolyte volumes (using the previously determined values of D_m^{IV} and the fitted polynomial function in Figure 6). The theoretical prediction of $c_v^{IV}(t)$, when variation in the electrolyte volume is considered (red line), coincide well with experiment data, Figure 7(a). In contrast, in the case where the electrolyte volume is kept as constant, the theoretical prediction of $c_v^{IV}(t)$ (green line) is approximately constant (variation of only 1.26% after 50 h) and consequently, significantly deviates from experimental data. Thus, the VO^{2+} concentration on "vanadium" side is significantly (approximately by 99%) affected by dilution induced by water transport rather than by the diffusion of VO^{2+} species across Nafion™ 424 membrane.

Thereafter, only the value of D_m^{IV} obtained by considering the variation in electrolyte volume ($D_m^{IV} = 1.59 \times 10^{-12}$ $m^2.s^{-1}$) will be used and the corresponding estimated average molar flux of VO^{2+} (J_{Dm}^{IV}) is equal to 2.38×10^{-8} $mol.s^{-1}$.

Theoretical and experimental temporal evolutions of H^+ concentration on "vanadium" and "sulfuric acid" sides are showed in Figure 8(a) and (b) respectively. Both theoretical and experimental results indicate a decrease in acidity on "vanadium" side (Figure 8 (a)), which is due to the dilution caused by the water coming from "sulfuric acid" side by osmosis. On "sulfuric acid" side, water transport leads to increase H^+ concentration as indicated in Figure 8 (b). The theoretical and experimental curves coincide well for H^+ concentration in both sides with a relative error less than 3 % at each time. This validates the assumptions made and the accuracy of the polynomial models used to fit the variation in electrolyte volume in both sides.

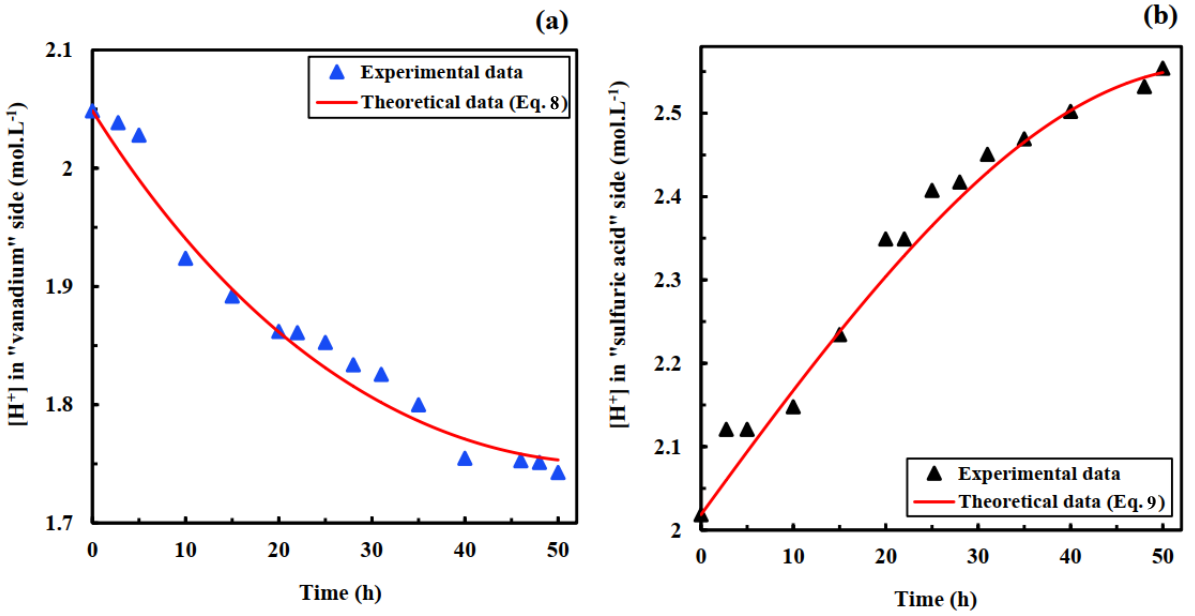

Figure 8: Theoretical (red lines) and experimental (black and blue triangles) temporal evolution of H^+ concentration on "vanadium" (a) and "sulfuric acid" (b) side; flowrate = 40 $L.h^{-1}$, initial conditions on "Vanadium" side: $V_v(0)$ = 200 mL, $[H_2SO_4]$ = 2.05 $mol.L^{-1}$, $[VO^{2+}]$ = 1.69 $mol.L^{-1}$; initial conditions on "sulfuric acid" side: $V_s(0)$ = 200 mL, $[H_2SO_4]$ = 2.02 $mol.L^{-1}$.

4.2.Experiment under galvanostatic polarization (case B)

The same experiment as above is carried out but by polarizing the electrodes of the electrochemical reactor, under galvanostatic control and the applied current I = 0.2 A. The positive electrode, i.e. the anode, is the electrode located on the "vanadium" side which is now called posolyte side. The negative electrode, i.e. the cathode, is the electrode located on the "sulfuric acid" side which is now called negolyte side, Figure 1 and 3.

The variation of electrolyte volume on both sides is showed in Figure 9. The volume of electrolyte decreases by ~19% in negolyte while it increases by ~14.5% in posolyte. In the posolyte, water is electrochemically consumed by Rx. II and III, oxidized by Rx. V and dragged by diffusion and migration fluxes of cationic species (VO^{2+}, VO_2^+, H^+, and also V^{3+}, V^{2+} coming from the negolyte by diffusion) across the membrane. In the negolyte, water is electrochemically produced by the reactions Rx. VII (reduction of VO_2^+) and VIII (reduction of VO^{2+}). However, in the negolyte, the concentrations of VO_2^+ and VO^{2+} remains very low

(<0.005 M) and consequently the amount of water produced by Rx. VII and VIII is negligible. Water is transported by osmosis from the negolyte to the posolyte. Based on the trends of variations in electrolyte volume indicated in Figure 9, it can be concluded that the loss of water in posolyte by non-osmotic processes occurring within the reactor (including Rx. II, III and V, transport mechanism of VO^{2+}, VO_2^+ V^{3+}, V^{2+}, and H^+ with bond water) is lower than the water supply by osmosis process. Therefore, the osmosis can be considered as the prevailing mechanism of electrolyte volume variation in posolyte and negolyte.

The electrolyte volume variation in negolyte is ~31% higher than that recovered in posolyte (100×(19/14.5-1)); this is 2.4 times higher than the discrepancy observed when experiment is conducted without polarization (~13%, Figure 6). This is explained by the electrochemical consumption of water in posolyte (electrochemical oxidation of VO^{2+} and V^{3+} in 1:1 mol ratio, Rx. II and III, and the oxidation of water, Rx. V, if $I_{lim,p(II,III,IV)} < I$) in addition to the evaporation and vanadium solvation as reported for the case A.

As in case A, second order polynomial functions are used to fit the electrolyte volume variation in the two storage tanks, thus providing terms that best describes the volume change of specific storage tank (Figure 9).

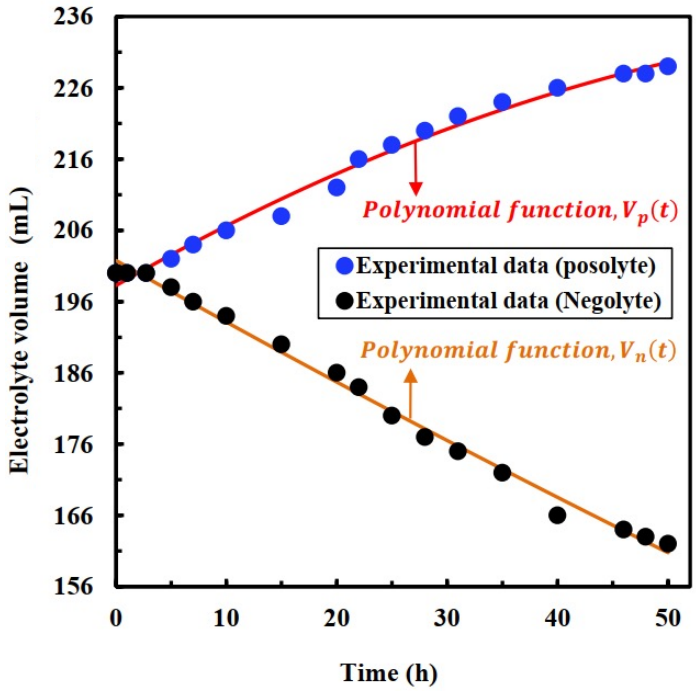

Figure 9: Temporal electrolyte volume change in posolyte and negolyte side (disks) and the corresponding polynomial fit curves (solid lines); flowrate = 40 L/h, I = 0.2 A, S_e = 20 cm^2, initial conditions in posolyte: $V_p(0)$ = 200 mL, [H_2SO_4] = 2.02 mol.L^{-1}, [VO^{2+}] = 1.69 mol.L^{-1}; initial conditions in negolyte: $V_n(0)$ = 200 mL; [H_2SO_4]: 2.01 mol.L^{-1}.

The Faradaic yield (η_F) of the electrochemical oxidation of VO^{2+} is calculated from the following relationship:

$$\eta_F = \frac{c_p^{IV}(t=0)V_p(t=0)F}{It_f}, \quad (35)$$

where t_f = ~46 h is the time from which VO^{2+} is no longer detected in the posolyte (Figure 10(a)). The obtained value of η_F is ~98%, indicating that most of the applied current was effectively used for the VO^{2+} ions conversion into VO_2^+. This efficiency is due to the low applied current and the high electrode surface area used in this study, resulting in a very low current density of 10 mA.cm^{-2}.

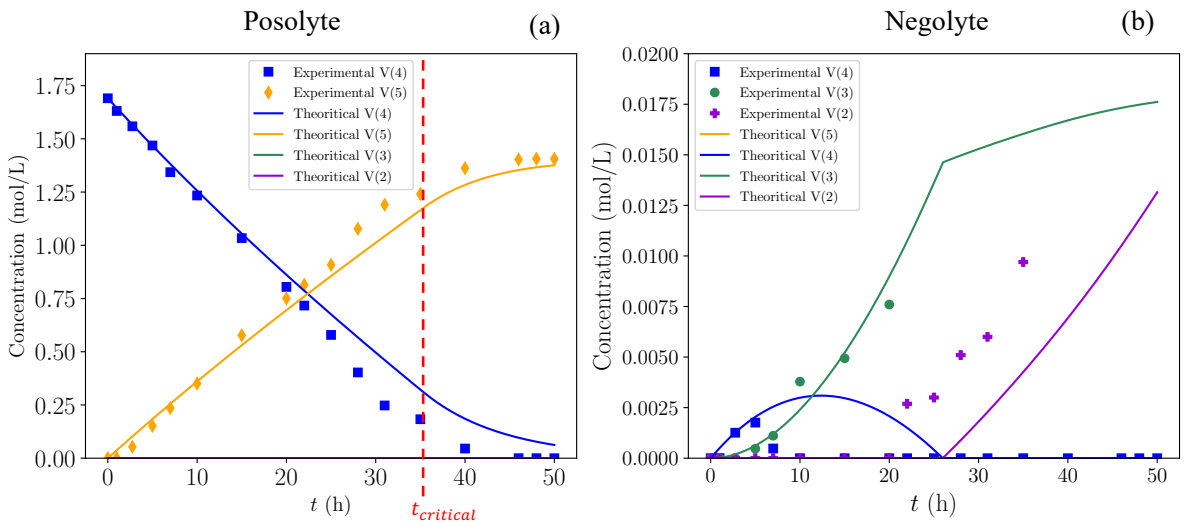

Figure 10: Theoretical (solid lines) and experimental (markers) temporal evolutions of vanadium species concentrations in posolyte (a) and in negolyte (b), V(2) = V^{2+} (purple), V(3) = V^{3+} (green), V(4) = VO^{2+} (blue), V(5) = VO_2^+ (orange). The vertical red dashed line in (a) indicates the critical time $t_{critical}$ (~35 h) which corresponds to the condition $I = I_{lim}^{IV}$; flowrate = 40 L/h, I = 0.2 A, S_e = 20 cm^2, initial conditions in posolyte: $V_p(0)$ = 200 mL, [H_2SO_4] = 2.02 $mol.L^{-1}$, [VO^{2+}] = 1.69 $mol.L^{-1}$; initial conditions in negolyte: $V_n(0)$ = 200 mL; [H_2SO_4]: 2.01 $mol.L^{-1}$.

Figure 10(a) shows the experimental and theoretical temporal evolution of VO^{2+} and VO_2^+ concentrations in the posolyte. The theoretical curves were obtained from numerical resolution of Eq. 10 using parameter values listed in Table 1. Note that for D_m^{IV}, the value obtained in the previous case (experiment without polarization, case A) was used. The theoretical values of V^{3+} and V^{2+} concentrations are also provided. According to this figure, the concentration of VO^{2+} decreases in posolyte over time, this is mainly due to the electrochemical oxidation (Rx. II) and the dilution caused by water transfer. From 46 h, the VO^{2+} was no longer experimentally detected in the posolyte (complete electrochemical oxidation of VO^{2+}), while VO_2^+ began to be detected from 2.75 h and reached its maximum concentration value of ~1.4 $mol.L^{-1}$ when the electrochemical consumption of VO^{2+} is stopped at 46 h. The experimental and theoretical concentration of VO_2^+ in posolyte show negligible overall deviation, with a higher deviation of ~14% observed at 31 h. The agreement between the experimental concentration of VO^{2+} and

the theoretical ones seems very good between 0 and 22 h (relative error < 9%), while a significant deviation is observed from 25 to 50 h. As expected, the predicted concentration of V^{2+} and V^{3+} in posolyte are very low and negligible compared to the concentration of VO^{2+} and VO_2^+. Experimentally, neither V^{2+} nor V^{3+} are detected in posolyte.

Table 1
Parameter values used for the numerical resolution of case B.

Vanadium ion	VO_2^+ (i=V)	VO^{2+} (i=IV)	V^{3+} (i=III)	V^{2+} (i=II)
Effective diffusion coefficient D_m^i ($\times 10^{-12}$ m^2/s)	1.7 [16]	1.6	5.9 [16]	3.1 [39]
Mass transfer coefficient k_c^i ($\times 10^{-6}$ m/s) [36]	3.6	3.4	2.2	4.4

Simultaneously to the electrochemical and chemical reactions occurring on the posolyte side, VO^{2+} and VO_2^+ are transported across membrane towards the negative side by diffusion and migration. The corresponding average mass flux of VO^{2+}, $J_{(D,M)_m}^{IV}$ (Eq. 14), is equal to 2.95 $\times 10^{-8}$ mol.s^{-1}, which is approximately 24% higher than the value of $J_{D_m}^{IV}$ found when experiment was conducted without polarization (migration = 0). This increase is attributed to the additional flux of VO^{2+} caused by migration. Using the proposed modelling in section 3.2, the part of diffusive ($J_{D_m}^{IV}$) and migration ($J_{M_m}^{IV}$) flux is estimated to be equal to 2.68×10^{-8} and 0.27×10^{-8} mol.s^{-1}, respectively, indicating that the total flux of VO^{2+} across the membrane is 91% controlled by diffusion mechanism and the migration part corresponds approximately 9% of the total flux (because of the presence of 2 M sulfuric acid electrolyte). This increase in overall amount of crossed-over VO^{2+} raises the production of the total amount of vanadium species on negolyte side as also reported by Oh et al. [40]. Also note the very good quantitative agreement between the values of $J_{(D,M)_m}^{IV}$ measured experimentally and determined numerically.

On the negolyte side, there are several electrochemical reactions including reduction of VO_2^+, VO^{2+} and V^{3+} to form VO^{2+}, V^{3+} and V^{2+}, respectively. These vanadium species concentrations are determined by UV-visible as described in section 2.2. Figure 10(b) displays the theoretical and experimental temporal evolution of vanadium species concentration in negolyte. The theoretical curves were obtained from numerical resolution of Eq. 11 using parameter values listed in Table 1. It is observed at 2.75 h that VO^{2+} appears in negolyte because of the crossover phenomenon occurring across Nafion^{TM} 424 membrane. Once inside the negolyte, VO^{2+} is electrochemically reduced to V^{3+} according to Rx. VIII, which in turn is electrochemically reduced to form V^{2+} according to Rx. IX. The theoretical and experimental curves show approximately similar trends, especially for V^{3+} and V^{2+} concentrations indicating their increase over time in negolyte. For V^{3+}, a very good agreement is observed, the average relative gap between experimental and theoretical values is lower than 13.3%. After 22 h, the concentration of V^{3+} is not deduced from the absorbance at 401 nm because of the overlap with the signal of V^{2+} which starts to appear in negolyte. The model also predicts the delayed appearance of V^{2+} with a production starting from t~26 h. After 26 h, the average production rate of V^{2+} predicted by the model ($\overline{dc_n^{II}/dt}$) deviates by less than 8% from the experimental one. Concerning VO^{2+}, experimental results indicate that it initially accumulates in the negolyte, its concentration reaches a maximum at t~5 h then decreases and VO^{2+} is no longer detected after 10 h. The model predicts the same temporal evolution but with a longer time from which the electrolyte is completely depleted of it. No VO_2^+ specie is detected in negolyte during experiment. The theoretical model is agreement with the latter result by predicting a negligible VO_2^+ concentration (less than 10^{-7} mol/L).

In order to analyse more precisely the evolution of negolyte composition, the deconvolution process (section 2.3) is applied to the UV-vis spectra. The thus extracted spectra and the raw spectra (baseline corrected) are plotted on the same graphs for several times in Figure 11. In

Figure 11(a-b), from 5 h to 7 h, peaks were easily separated to provide different single signals centered at ~400 (V^{3+}), ~610 (V^{3+} and V^{2+}) and ~760 nm (VO^{2+}) and the evolution of their respective amplitudes shows that the concentration of VO^{2+} decreases and that the concentration of V^{3+} increases.

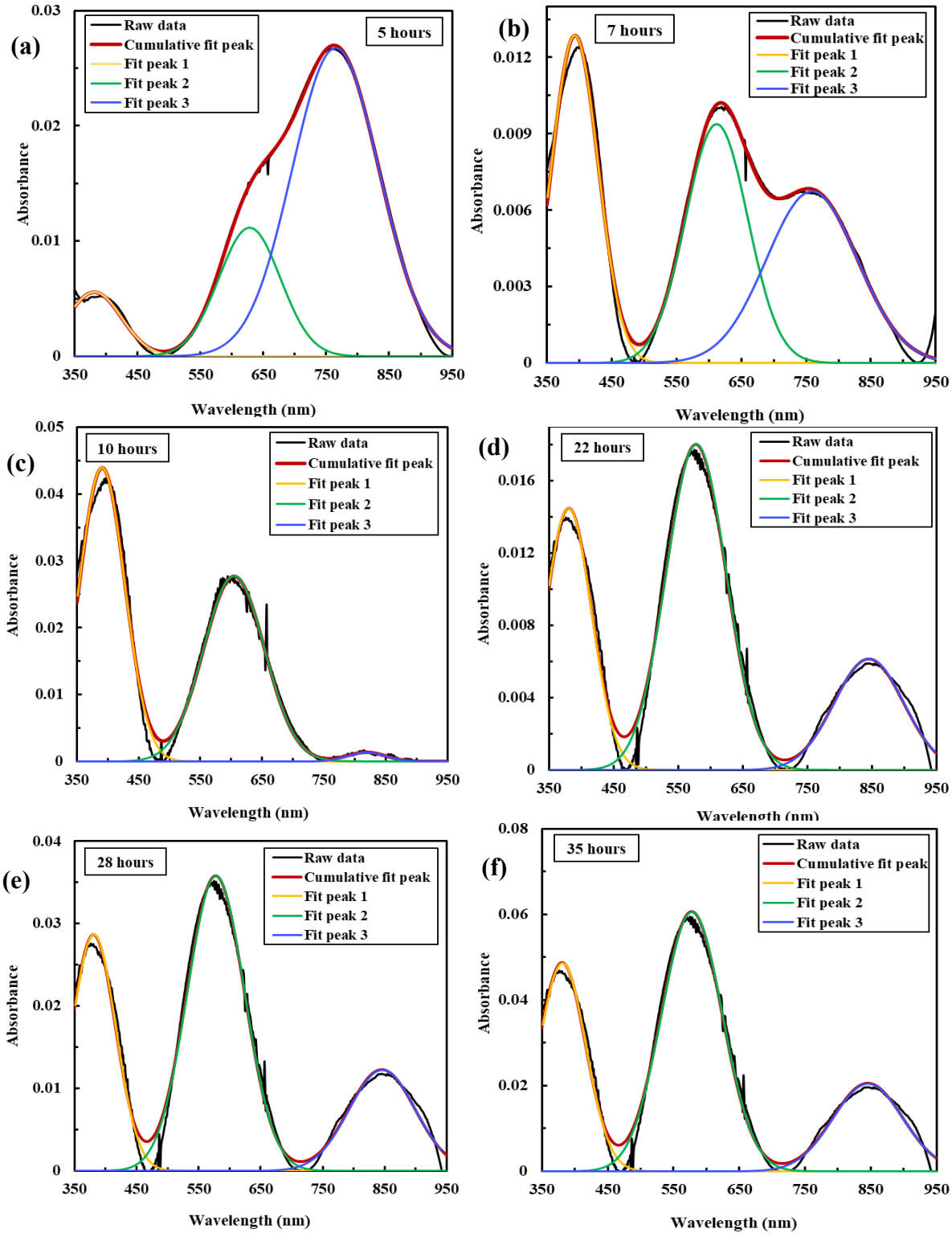

Figure 11: Deconvolution of UV-vis spectra obtained in negolyte after an electrolysis time of 5 h (a), 7 h (b), 10 h (c), 22 h (d), 28h (e) and 35h (f). Only 3 Gaussian signals out of the 4 sought (around 400, 610, 760 and 855 nm, see section 2.3) are shown because the fitting process systematically returned one Gaussian signal/function with negligible amplitude with these experiment data.

However, no peak was found at 760 nm (VO^{2+}) from 10 to 50 h (Figure 11(b-f)) and the spectra from 22 to 35 h (Figure 11(d-f)) correspond in part to that of V^{2+} since a peak is observed near 855 nm. Consequently, from 10 h and up to the end of the experiment (50 h), UV-vis spectra show that the negolyte contains mainly V^{3+} and V^{2+}. The amplitude of extracted signal centered at ~855 nm, thus corresponding to V^{2+}, increases over time: from ~0.006 at 22 h (Figure 11(d)), ~0.01 at 28 h (Figure 11(e)) to ~0.02 at 35 h (Figure 11(f)). In Figure 11(c) (10 h), the small peak centered at 825 nm (from the deconvolution process used) cannot be attribute to V^{2+} or VO^{2+} because this wavelength does not correspond to the known characteristic wavelengths of the vanadium species (855 nm and 760 nm). The temporal evolution of the amplitude of the two other signals, centered at ~400 and ~600 nm, is more complicated to analyse since they contain the contribution of both species V^{3+} and V^{2+}. After a decrease from 10 to 22 h, the amplitude of both signals increases over time. To sum up, this deduced evolution of negolyte composition, based on processed UV-vis spectra, is in qualitative agreement with the prediction of the theoretical model showing an enrichment in V^{3+} from the start of the experiment, a complete depletion in VO^{2+} after 10 h and a delayed production and enrichment in V^{2+} starting from 22 h.

In Figure 10(b), the theoretical concentration curves are “broken” (discontinuity of the first derivate) because the self-discharge reactions are considered instantaneous. To clearly show this effect, several simulations were carried out by varying the value of the reaction rate constant ($k_{i,j}$) from 0 to 1 $m^3.mol^{-1}.s^{-1}$. The corresponding temporal evolutions of vanadium species concentrations are shown in Figure 12. In Figure 12(a), by assuming no self-discharge reactions ($k_{i,j} = 0$), the model predicts no depletion of VO^{2+} but instead an enrichment followed by a kind of steady state where the consumption of VO^{2+} by electrochemical reduction is compensated by the production from the electrochemical reduction of incoming VO_2^+. Besides,

VO_2^+ penetrates progressively in the negolyte with an increasing rate (due to its accumulation in the posolyte) up to ~20-30 h from when its electrochemical conversion rate to VO^{2+} becomes significant (see the variation in slope of the orange curve in Figure 12(a)). The electrochemical reduction of VO^{2+} leads to the progressive formation of V^{3+} which is itself reduced electrochemically to V^{2+} which also gradually invades the negolyte.

By enabling self-discharge reactions, between VO_2^+ and V^{2+}, between VO^{2+} and V^{2+} and between VO_2^+ and V^{3+}, as shown in Figures 12(b-f), the concentrations of VO_2^+ and V^{2+} are first affected; they decrease with the value of the reaction rate constant ($k_{i,j}$) because these species are not produced (or renewed) by the self-discharge reactions (Rx. X-XII). The concentration of VO_2^+ even converges to 0 at all times when the reaction rate constant increases. The same is observed for V^{2+} but only for t < ~26 h. After ~26 h, for high values of the reaction rate constant ($k_{i,j}$ > 0.1 $m^3.mol^{-1}.s^{-1}$), the concentration of V^{2+} becomes positive with an almost constant production rate. The self-discharge reactions boost the production of V^{3+}, as shown by comparing Figure 12(a) and Figures 12(b-f).

As for VO^{2+}, increasing the reaction rate constant leads to promoting its consumption by V^{2+} (Rx. XII). There is a competition between VO^{2+} crossover, electrochemical reduction of VO^{2+} and chemical consumption by self-discharge reaction (Rx XII) over time. For a sufficiently high reaction rate constant ($k_{i,j}$ > 0.1 $m^3.mol^{-1}.s^{-1}$), the curve showing the concentration of VO^{2+} as a function of time remains unchanged, exhibits a maximum value at ~12 h and tends towards 0 after ~26 h. Before 26 h, the production rate (crossover of VO^{2+} and electrochemical production by reduction of VO_2^+) is high enough to compensate the chemical consumption by V^{2+} while after 26 h, it is no longer high enough to compensate the chemical action of V^{2+} which is significantly produced owing to the enrichment in V^{3+}. This is shown for not too high values of the reaction rate constant in Figures 12(c-d). In these latter figures,

the area below the concentration curves for VO^{2+} and V^{2+}, and below their crossing point ~26 h (zone shown in Figure 12(c) by the grey hatched area), shrinks when the reaction rate constant is increased. In the limit of high reaction rate constants, this area vanishes and this results in "broken" curves as shown in Figure 12(e-f). In Figures 12(e-f), the break in the production rate of V^{3+} at ~26 h is due to the full depletion of VO^{2+} from t ~26 h which prevents V^{3+} production by self-discharge reaction between V^{2+} and VO^{2+} (Rx. XII). However, V^{3+} (and V^{2+}) is still electrochemically produced from VO_2^+. This transition is also shown with moderate values of the reaction rate constant (and thus smooth curves), e.g. in Figure 12(c), where the decrease in the rate of V^{3+} production is directly correlated with the decrease in the concentration of VO^{2+} after 26 h. From Figures 12(e-f), it is demonstrated that the model prediction no longer depends on the value of the reaction rate constant from a value of 0.1 $m^3.mol^{-1}.s^{-1}$. This analysis shows that the self-discharge reactions must be taken into account, as instantaneous reactions, in the model to correctly predict the main phenomena observed experimentally (complete depletion of VO^{2+} and delayed appearance of V^{2+}).

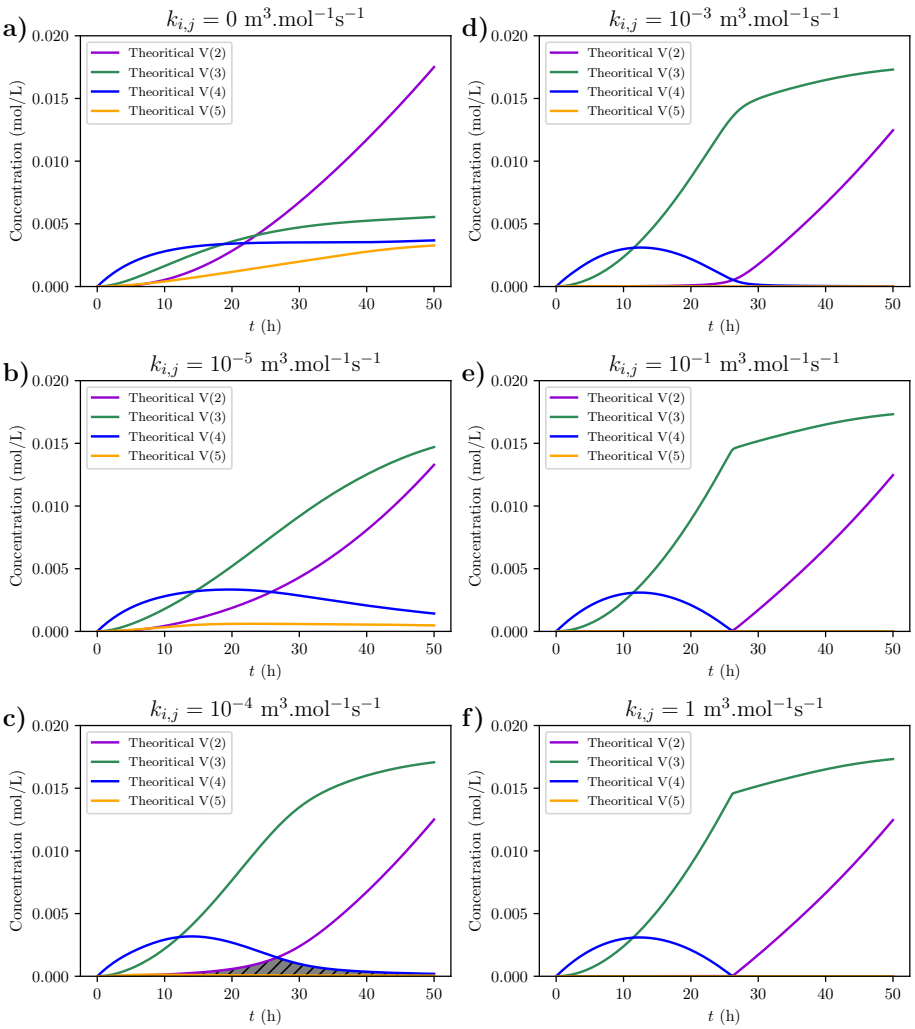

Figure 12: Theoretical temporal evolutions of the concentrations of vanadium species in the negolyte for various values of the reaction rate constant $k_{i,j}$ of self-discharge reactions, V(2) = V^{2+} (purple), V(3) = V^{3+} (green), V(4) = VO^{2+} (blue), V(5) = VO_2^+ (orange). I = 0.2 A, S_e = 20 cm^2, initial conditions in posolyte: $V_p(0)$ = 200 mL, [VO^{2+}] = 1.69 mol.L^{-1}; initial conditions in negolyte: $V_n(0)$ = 200 mL; [VO^{2+}] = 0.

As for change in amount of H^+ in respective electrolyte, Eq. 12 (associated to the corresponding $J_{p,elec}^{H^+}$) and Eq. 13 (associated to the corresponding $J_{n,elec}^{H^+}$) are numerically solved to estimate the theoretical change in the concentration of H^+ in posolyte and negolyte respectively. Figure 13 shows theoretical and experimental curves of acidity variation in posolyte and negolyte. For the posolyte, the trend of experimental and theoretical curve is approximately the same, according to which the H^+ concentration increases linearly from t = 0 to t = ~35 h. The time t = ~35 h corresponds approximately to the critical time "$t_{critical}$"

(indicated in Figure 10(a)), i.e. the time at which $I_{lim,p(II,III,IV)} = I$ and from which the electrochemical oxidation of VO^{2+} is limited by mass transfer. After 35 h, the H^+ concentration increases again but with a low rate which explains the change in the trend of the curve from ~35 h. Indeed, before $t_{critical}$, 1 mol of electron leads to the production of 2 mol of H^+ (Rx. II), while after $t_{critical}$ only 1 mol of H^+ is produced per electron, i.e. a decrease of 50% in the H^+ production rate.

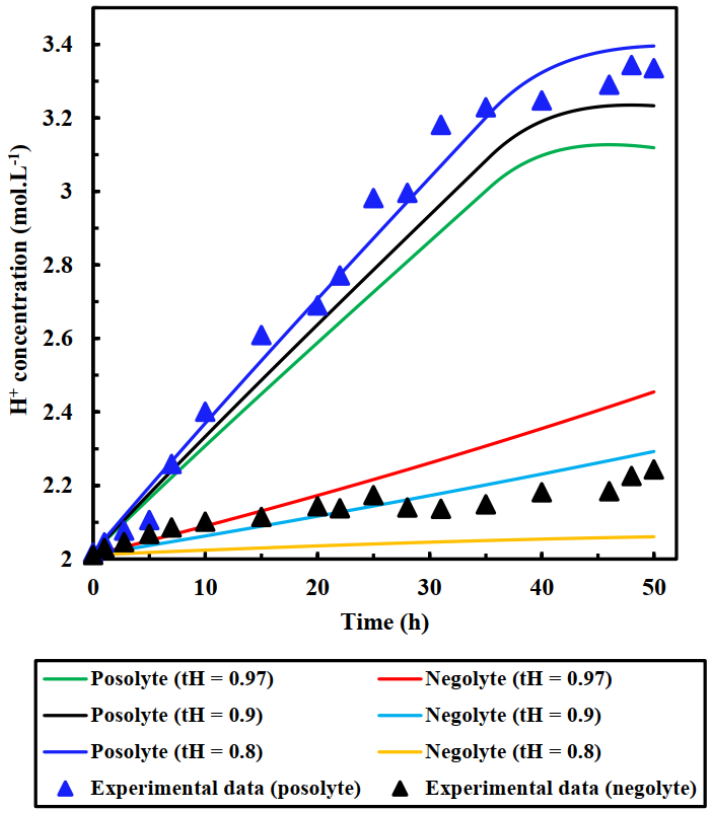

Figure 13: Theoretical (solid lines) and experimental (blue and black triangles) temporal evolutions of H^+ concentration in posolyte and negolyte, t_H: transference number (t^{H^+}); flowrate = 40 L/h, I = 0.2 A, S_e: electrode active area (20 cm^2), initial conditions in posolyte: $V_p(0)$ = 200 mL, $[H_2SO_4]$ = 2.02 $mol.L^{-1}$, $[VO^{2+}]$ = 1.69 $mol.L^{-1}$; initial conditions in negolyte: $V_n(0)$ = 200 mL, $[H_2SO_4]$ = 2.01 $mol.L^{-1}$.

In the negolyte, both theoretical and experimental data exhibit an increase in H^+ concentration over time. However, it is observed that the experimental H^+ concentration in negolyte is increased by 11% from t = 0 to t = 50 h, while the theoretical ones increased by

20% in the same time span for t_H = 0.97. The observed increase in the concentration of H^+ in the negolyte can be attributed mainly to the migration of H^+ to balance charges and the water transport.

Additionally, it is observed that the theoretical concentration of H^+ strongly depends on transference number. According to the Figure 13, theoretical and experimental curves do not match well when the value of the transference number t^{H^+} is 0.97, while a satisfactory agreement is observed when a lower value is employed to compute the theoretical prediction. Indeed, such a decrease in selectivity performance of the Nafion membrane can be observed when using concentrated solutions. This is quantitatively shown in the work of Okada et al. [41] (for Nafion 117), where authors measured the proton transference number as a function of proton mole fraction in the membrane. In the present study, there is a proton mole fraction difference between both sides: ~0.55 and ~0.99 for negolyte and posolyte respectively. By selecting an average value of 0.77 and by using the data from Okada et al. [41], an average proton transference number of 0.93 is deduced. The corresponding obtained relative error of 7% ((1-0.93)/1, where 1 is the value of proton transference number when proton mole fraction = 1, [41]) is close to relative error graphically estimated (~7.2%) from Figure 13 ((0.97-0.90)/0.97) to match experimental data to the theoretical prediction. Therefore, this analysis shows that the temporal evolution of proton concentration, or acidity, is affected by electrolyte composition.

Conclusions

In this study, vanadium crossover as well as the monitoring of the electrolyte composition are investigated using an electrochemical press filter reactor integrating Nafion™ 424 membrane. Various experiments are conducted by monitoring vanadium ions (VO_2^+, VO^{2+},

V^{3+} and V^{2+}), H^+, as well as water intercompartment transfer, without polarization and under galvanostatic polarization. Under galvanostatic polarization (10 mA/cm^2), it is observed that the average mass flux of VO^{2+} through the membrane, towards the negolyte side, is increased by 24% (compared to the case without polarization) because of the migration effect induced by the electric field. This shows that migration transport must be taken into account to predict correctly the crossover rate.

In parallel, a model was derived, which considers the mass balance of the various species in the electrolytes and in the membrane; the model takes into account simultaneously:

- the transport (diffusion and migration) of the species in the membrane
- the partitioning of the applied current between all possible electrochemical reactions (including oxidation and reduction of water)
- the self-discharge reactions (assumed fast)
- the variation in electrolyte volumes.

The model enables to predict the temporal evolution of electrolyte composition. The overall agreement between model predictions and experiment measurements is satisfactory for both H^+ and vanadium species concentration. Note that the derived model can be used with other membranes, providing that the effective diffusion coefficients and the water transfer rate are determined by diffusion experiments (without polarization); the other required membrane parameters (thickness, conductivity and transference number of protons) being known from the supplier.

Thus, the derived model is proposed for the prediction of H^+ and vanadium species concentrations on both sides as a function of time (which corresponds to a given SoC) in a VRFB during charge/discharge cycles. Additionally, such a model is also well suited to predict energy loss coming from vanadium cross-over. The adaptation of the derived model to a VRFB operating under galvanostatic condition will be treated in a future work.

Declaration of Competing Interest

The authors declare that they have no known competing financial interests or personal relationships that could have appeared to influence the work reported in this paper.

Acknowledgments

The funding from Région Occitanie (Projet DEMO TOUT VA, N°92810/21016156) is gratefully acknowledged.

References

[1] L. Zeng, T.S. Zhao, L. Wei, H.R. Jiang, M.C. Wu, Anion exchange membranes for aqueous acid-based redox flow batteries: Current status and challenges, Appl. Energy 233–234 (2019) 622–643. https://doi.org/10.1016/j.apenergy.2018.10.063.

[2] M. Skyllas-Kazacos, G. Kazacos, G. Poon, H. Verseema, Recent advances with UNSW vanadium-based redox flow batteries, Int. J. Energy Res. 34 (2010) 182–189. https://doi.org/10.1002/er.1658.

[3] G. Kear, A.A. Shah, F.C. Walsh, Development of the all-vanadium redox flow battery for energy storage: a review of technological, financial and policy aspects, Int. J. Energy Res. 36 (2012) 1105–1120. https://doi.org/10.1002/er.1863.

[4] J.H. Vinco, A.E.E. da C. Domingos, D.C.R. Espinosa, J.A.S. Tenório, M. dos P.G. Baltazar, Unfolding the Vanadium Redox Flow Batteries: An indeep perspective on its

components and current operation challenges, J. Energy Storage 43 (2021) 103180. https://doi.org/10.1016/j.est.2021.103180.

[5] M. Dieterle, P. Fischer, M.-N. Pons, N. Blume, C. Minke, A. Bischi, Life cycle assessment (LCA) for flow batteries: A review of methodological decisions, Sustain. Energy Technol. Assess. 53 (2022) 102457. https://doi.org/10.1016/j.seta.2022.102457.

[6] A. Tang, J. Bao, M. Skyllas-Kazacos, Studies on pressure losses and flow rate optimization in vanadium redox flow battery, J. Power Sources 248 (2014) 154–162. https://doi.org/10.1016/j.jpowsour.2013.09.071.

[7] A. Parasuraman, T.M. Lim, C. Menictas, M. Skyllas-Kazacos, Review of material research and development for vanadium redox flow battery applications, Electrochimica Acta 101 (2013) 27–40. https://doi.org/10.1016/j.electacta.2012.09.067.

[8] C. Ding, H. Zhang, X. Li, H. Zhang, C. Yao, D. Shi, Morphology and Electrochemical Properties of Perfluorosulfonic Acid Ionomers for Vanadium Flow Battery Applications: Effect of Side-Chain Length, ChemSusChem 6 (2013) 1262–1269. https://doi.org/10.1002/cssc.201300014.

[9] Q. Luo, L. Li, Z. Nie, W. Wang, X. Wei, B. Li, B. Chen, Z. Yang, In-situ investigation of vanadium ion transport in redox flow battery, J. Power Sources 218 (2012) 15–20. https://doi.org/10.1016/j.jpowsour.2012.06.066.

[10] T. Sukkar, M. Skyllas-Kazacos, Modification of membranes using polyelectrolytes to improve water transfer properties in the vanadium redox battery, J. Membr. Sci. 222 (2003) 249–264. https://doi.org/10.1016/S0376-7388(03)00316-8.

[11] K. Lourenssen, J. Williams, F. Ahmadpour, R. Clemmer, S. Tasnim, Vanadium redox flow batteries: A comprehensive review, J. Energy Storage 25 (2019) 100844. https://doi.org/10.1016/j.est.2019.100844.

[12] A. Tang, J. Bao, M. Skyllas-Kazacos, Dynamic modelling of the effects of ion diffusion and side reactions on the capacity loss for vanadium redox flow battery, J. Power Sources 196 (2011) 10737–10747. https://doi.org/10.1016/j.jpowsour.2011.09.003.

[13] J. Sun, D. Shi, H. Zhong, X. Li, H. Zhang, Investigations on the self-discharge process in vanadium flow battery, J. Power Sources 294 (2015) 562–568. https://doi.org/10.1016/j.jpowsour.2015.06.123.

[14] T. Sukkar, M. Skyllas-Kazacos, Water transfer behaviour across cation exchange membranes in the vanadium redox battery, J. Membr. Sci. 222 (2003) 235–247. https://doi.org/10.1016/S0376-7388(03)00309-0.

[15] T. Mohammadi, S.C. Chieng, M. Skyllas Kazacos, Water transport study across commercial ion exchange membranes in the vanadium redox flow battery, J. Membr. Sci. 133 (1997) 151–159. https://doi.org/10.1016/S0376-7388(97)00092-6.

[16] J. Xi, Z. Wu, X. Teng, Y. Zhao, L. Chen, X. Qiu, Self-assembled polyelectrolyte multilayer modified Nafion membrane with suppressed vanadium ion crossover for vanadium redox flow batteries, J. Mater. Chem. 18 (2008) 1232–1238. https://doi.org/10.1039/B718526J.

[17] S. Lu, C. Wu, D. Liang, Q. Tan, Y. Xiang, Layer-by-layer self-assembly of Nafion–[CS–PWA] composite membranes with suppressed vanadium ion crossover for vanadium redox flow battery applications, RSC Adv. 4 (2014) 24831–24837. https://doi.org/10.1039/C4RA01775G.

[18] L. Zhang, L. Ling, M. Xiao, D. Han, S. Wang, Y. Meng, Effectively suppressing vanadium permeation in vanadium redox flow battery application with modified Nafion membrane with nacre-like nanoarchitectures, J. Power Sources 352 (2017) 111–117. https://doi.org/10.1016/j.jpowsour.2017.03.124.

[19] T. Wang, J. Han, K. Kim, A. Münchinger, Y. Gao, A. Farchi, Y.-K. Choe, K.-D. Kreuer,

C. Bae, S. Kim, Suppressing vanadium crossover using sulfonated aromatic ion exchange membranes for high performance flow batteries, Mater. Adv. 1 (2020) 2206–2218. https://doi.org/10.1039/D0MA00508H.

[20] X. Lou, D. Yuan, Y. Yu, Y. Lei, M. Ding, Q. Sun, C. Jia, A Cost-effective Nafion Composite Membrane as an Effective Vanadium-Ion Barrier for Vanadium Redox Flow Batteries, Chem. – Asian J. 15 (2020) 2357–2363. https://doi.org/10.1002/asia.202000140.

[21] O. Nolte, I.A. Volodin, C. Stolze, M.D. Hager, U.S. Schubert, Trust is good, control is better: a review on monitoring and characterization techniques for flow battery electrolytes, Mater Horiz 8 (2021) 1866–1925. https://doi.org/10.1039/D0MH01632B.

[22] Y. Li, State-of-Charge Monitoring for Vanadium Redox Flow Batteries, in: Flow Batter., John Wiley & Sons, Ltd, 2023: pp. 627–640. https://doi.org/10.1002/9783527832767.ch27.

[23] C. Sun, J. Chen, H. Zhang, X. Han, Q. Luo, Investigations on transfer of water and vanadium ions across Nafion membrane in an operating vanadium redox flow battery, J. Power Sources 195 (2010) 890–897. https://doi.org/10.1016/j.jpowsour.2009.08.041.

[24] D. You, H. Zhang, C. Sun, X. Ma, Simulation of the self-discharge process in vanadium redox flow battery, J. Power Sources 196 (2011) 1578–1585. https://doi.org/10.1016/j.jpowsour.2010.08.036.

[25] C. Weidlich, F. Lulay, M. Wieland, Feasibility study of amperometric and electrochemical quartz crystal microbalance measurements for in situ state of charge monitoring in vanadium flow batteries, J. Electrochem. Sci. Eng. 13 (2023) 739–751.

[26] V.I. Vlasov, M.A. Pugach, D.S. Kopylova, A.V. Novikov, N.A. Gvozdik, A.A. Mkrtchyan, A.I. Davletkhanov, Y.G. Gladush, F.M. Ibanez, D.A. Gorin, K.J. Stevenson, In situ state of health vanadium redox flow battery deterministic method in cycling operation for

battery capacity monitoring, J. Power Sources 584 (2023) 233600. https://doi.org/10.1016/j.jpowsour.2023.233600.

[27] M. Skyllas-Kazacos, L. Goh, Modeling of vanadium ion diffusion across the ion exchange membrane in the vanadium redox battery, J. Membr. Sci. 399–400 (2012) 43–48. https://doi.org/10.1016/j.memsci.2012.01.024.

[28] A. Tang, J. Bao, M. Skyllas-Kazacos, Thermal modelling of battery configuration and self-discharge reactions in vanadium redox flow battery, J. Power Sources 216 (2012) 489–501. https://doi.org/10.1016/j.jpowsour.2012.06.052.

[29] K. Oh, M. Moazzam, G. Gwak, H. Ju, Water crossover phenomena in all-vanadium redox flow batteries, Electrochimica Acta 297 (2019) 101–111. https://doi.org/10.1016/j.electacta.2018.11.151.

[30] M. Cecchetti, F. Toja, A. Casalegno, M. Zago, A comprehensive experimental and modelling approach for the evaluation of cross-over fluxes in Vanadium Redox Flow Battery, J. Energy Storage 68 (2023) 107846. https://doi.org/10.1016/j.est.2023.107846.

[31] W.-J. Zou, Y.-B. Kim, S. Jung, Capacity fade prediction for vanadium redox flow batteries during long-term operations, Appl. Energy 356 (2024) 122329. https://doi.org/10.1016/j.apenergy.2023.122329.

[32] P.A. Boettcher, E. Agar, C.R. Dennison, E.C. Kumbur, Modeling of Ion Crossover in Vanadium Redox Flow Batteries: A Computationally-Efficient Lumped Parameter Approach for Extended Cycling, J. Electrochem. Soc. 163 (2015) A5244. https://doi.org/10.1149/2.0311601jes.

[33] Y.-S. Chou, S.-C. Yen, A. Arpornwichanop, B. Singh, Y.-S. Chen, Mathematical Model to Study Vanadium Ion Crossover in an All-Vanadium Redox Flow Battery, ACS Sustain. Chem. Eng. 9 (2021) 5377–5387. https://doi.org/10.1021/acssuschemeng.1c00233.

[34] L. Hao, Y. Wang, Y. He, Modeling of Ion Crossover in an All-Vanadium Redox Flow Battery with the Interfacial Effect at Membrane/Electrode Interfaces, J. Electrochem. Soc. 166 (2019) A1310. https://doi.org/10.1149/2.1061906jes.

[35] N. Hayer, M. Kohns, Thermodynamically Rigorous Description of the Open Circuit Voltage of Redox Flow Batteries, J. Electrochem. Soc. 167 (2020) 110516. https://doi.org/10.1149/1945-7111/ab9e85.

[36] R. El Hage, Study and optimization of a all vanadium redox flow battery, PhD Thesis, Université Toulouse III, Paul Sabatier, 2020. https://www.theses.fr/2020TOU30101.

[37] J. Zeng, C. Jiang, Y. Wang, J. Chen, S. Zhu, B. Zhao, R. Wang, Studies on polypyrrole modified nafion membrane for vanadium redox flow battery, Electrochem. Commun. 10 (2008) 372–375. https://doi.org/10.1016/j.elecom.2007.12.025.

[38] R.A. Elgammal, Z. Tang, C.-N. Sun, J. Lawton, T.A. Zawodzinski, Species Uptake and Mass Transport in Membranes for Vanadium Redox Flow Batteries, Electrochimica Acta 237 (2017) 1–11. https://doi.org/10.1016/j.electacta.2017.03.131.

[39] E. Agar, K.W. Knehr, D. Chen, M.A. Hickner, E.C. Kumbur, Species transport mechanisms governing capacity loss in vanadium flow batteries: Comparing Nafion® and sulfonated Radel membranes, Electrochimica Acta 98 (2013) 66–74. https://doi.org/10.1016/j.electacta.2013.03.030.

[40] K. Oh, S. Won, H. Ju, A comparative study of species migration and diffusion mechanisms in all-vanadium redox flow batteries, Electrochimica Acta 181 (2015) 238–247. https://doi.org/10.1016/j.electacta.2015.03.012.

[41] T. Okada, S. Møller-Holst, O. Gorseth, S. Kjelstrup, Transport and equilibrium properties of Nafion membranes with H + and Na + ions, J. Electroanal. Chem. 1–2 (1998) 137–145.